Journal of Computational Physics 229 (2010) 8888–8917

Contents lists available at ScienceDirect

Journal of Computational Physics

journal homepage: www.elsevier.com/locate/jcp

The backward phase flow and FBI-transform-based Eulerian Gaussian beams for the Schrödinger equation

Shingyu Leung [a], Jianliang Qian [b,*]

[a] Department of Mathematics, Hong Kong University of Science and Technology, Clear Water Bay, Hong Kong
[b] Department of Mathematics, Michigan State University, East Lansing, MI 48824, USA

ARTICLE INFO

Article history:
Received 8 March 2010
Received in revised form 11 August 2010
Accepted 12 August 2010
Available online 18 August 2010

Keywords:
Eulerian Gaussian beam
FBI transform
Reinitialization
Schrödinger
Backward phase flow

ABSTRACT

We propose the backward phase flow method to implement the Fourier–Bros–Iagolnitzer (FBI)-transform-based Eulerian Gaussian beam method for solving the Schrödinger equation in the semi-classical regime. The idea of Eulerian Gaussian beams has been first proposed in [12]. In this paper we aim at two crucial computational issues of the Eulerian Gaussian beam method: how to carry out long-time beam propagation and how to compute beam ingredients rapidly in phase space. By virtue of the FBI transform, we address the first issue by introducing the reinitialization strategy into the Eulerian Gaussian beam framework. Essentially we reinitialize beam propagation by applying the FBI transform to wavefields at intermediate time steps when the beams become too wide. To address the second issue, inspired by the original phase flow method, we propose the backward phase flow method which allows us to compute beam ingredients rapidly. Numerical examples demonstrate the efficiency and accuracy of the proposed algorithms.

1. Introduction

We consider the Schrödinger equation for a particle with unity mass

$$\begin{aligned} &-\imath\hbar U_t + V(x)U - \frac{\hbar^2}{2}\Delta U = 0, \quad x \in R^d, \ \ t > 0, \\ &U(x,0) = U_0(x), \end{aligned}$$

where $\imath = \sqrt{-1}$, V is real and smooth, $\hbar \equiv h/2\pi$ with h a small (scaled) Planck's constant, and U_0 is a compactly supported L^2 function, presumably highly oscillatory. Because the Schrödinger equation propagates oscillations of wavelength $\hbar$ in space and time, resolving such oscillations by direct finite difference methods requires many grid points per wavelength of $O(\hbar)$, which is costly in practice. As an alternative to obtain a numerical approximation capturing quantum effects, semi-classical methods are sought to link classical and quantum mechanics. In this paper, we further develop the Fourier–Bros–Iagolnitzer (FBI)-transform-based Eulerian Gaussian beam method, first proposed in [11], to compute the semiclassical solution for the Schrödinger equation.

The idea of *Eulerian Gaussian beam methods* has been first proposed in [12] to treat the Helmholtz equation. It can be naturally generalized to treat the Schrödinger equation as shown in [11]. To have an efficient Eulerian Gaussian beam method, there are three computational problems that one has to deal with. As the Eulerian Gaussian beam is formulated in phase space, the first computational problem is how to initialize beam propagation based on the initial data given in physical space. This problem has been successfully treated by using the FBI transform as originally proposed in [11].

* Corresponding author. Tel.: +1 517 353 6334; fax: +1 517 432 1562.
E-mail addresses: masyleung@ust.hk (S. Leung), qian@math.msu.edu (J. Qian).

0021-9991/$ - see front matter © 2010 Elsevier Inc. All rights reserved.
doi:10.1016/j.jcp.2010.08.015

The second problem is how to carry out long-time beam propagation. A simple analysis in [20] indicates that the width of a Gaussian beam can grow exponentially with time. An overly-extended Gaussian beam not only leads to large approximation errors in the Taylor expansions of phase and amplitude functions but also makes the final summation extremely expensive. Inspired by the reinitialization idea as first proposed in [20] in the context of Lagrangian Gaussian beams, we propose to reinitialize beam propagation whenever necessary in the FBI-transform-based Eulerian Gaussian beams, as our unique setup based on the FBI transform enables us to carry out reinitialization efficiently. In semi-classical approximation for quantum mechanics, it has been observed [18] that the semi-classical approximation breaks down for most initial states on a time scale very long compared to the "log time" ($\hat{t} = O(\log(\frac{1}{\hbar}))$). By using the reinitialization strategy we are able to compute valid semi-classical solutions beyond the log-time scale.

The third problem is how to compute beam ingredients efficiently in phase space so that the Eulerian Gaussian beam summation can be carried out rapidly. Inspired by the phase flow method [25], we propose the backward phase flow method to compute beam ingredients. The original phase flow method assumes that the domain in phase space under the phase flow is invariant so that the group property of the phase flow allows rapid interpolation on the invariant manifold. Our backward phase flow will not explicitly make such an assumption. Once we have a mapping generating the backward phase flow, we can apply this mapping repeatedly to generate beam ingredients for arbitrarily long time.

1.1. Related work

The idea underlying Gaussian beams is simply to build asymptotic solutions to partial differential equations concentrated on a single curve through the domain; this single curve is nothing but a ray as shown in [22]. The existence of such solutions has been known to the pure mathematics community since sometime in the 1960s [1], and these solutions have been used to obtain results on propagation of singularities in hyperbolic PDEs [9,22]. An integral superposition of these solutions can be used to define a more general solution that is not necessarily concentrated on a single curve. Gaussian beams can be used to treat pseudo-differential equations in a natural way, including Helmholtz and Schrödinger equations.

In geophysical applications, Gaussian beam superpositions have been used for seismic wave modeling [4] and for seismic wave migration [8]. The numerical implementations in these works are based on ray-centered coordinates which prove to be computationally inefficient [4,8]. More recently, based on [22,24] a purely Eulerian computational approach was proposed in [12] which overcomes some of these difficulties. To the best of our knowledge, the Eulerian Gaussian beam method proposed in [12] is the first efficient, successful Eulerian Gaussian beam framework; it can be easily applied to both high frequency waves and semi-classical quantum mechanics [11]. In [24] Lagrangian Gaussian beams are successfully constructed to simulate mountain waves, a kind of stationary gravity wave forming over mountain peaks and interfering with aviation. See [14] for Eulerian Gaussian beams for diffraction problems. See also [23,17] for some other recent works.

In quantum mechanics, some variants of Gaussian beams, such as frozen Gaussian beams and Gaussian wave packets, have been used to construct approximate solutions to the Schrödinger equation in the semi-classical regime [10,5,6]. However, these formulations were all based on the Lagrangian framework. In [11] we proposed an Eulerian formulation of Gaussian beams for the Schrödinger equation by generalizing the work in [12].

1.2. Contents

The rest of the paper is organized as follows. In Section 2, we outline the Lagrangian Gaussian beam formulation, describe the FBI transform for initializing beam propagation, summarize the Eulerian Gaussian beam formulation based on the FBI transform as developed in [11], and propose the beam reinitialization strategy to carry out long-time beam propagation in the Eulerian framework. In Section 3, we introduce the backward phase flow method to compute beam ingredients in phase space rapidly; the backward phase flow method couples nicely with the beam reinitialization strategy. In Section 4, we show that the FBI-transform-based Gaussian beam method yields an asymptotic solution to the Schrödinger equation. In Section 5, we show numerical examples to demonstrate the efficiency and accuracy of the algorithms.

2. Gaussian beams and the FBI transform

2.1. Lagrangian gaussian beams (LGB)

We consider the Schrödinger equation in the following form,

$$-\imath\hbar U_t + V(x)U - \frac{\hbar^2}{2}\Delta U = 0, \quad x \in R^d, \ t > 0, \tag{1}$$

$$U(x,0) = U_0(x), \tag{2}$$

where V is real and smooth, $\hbar \equiv h/2\pi$ with h a small (scaled) Planck's constant, and U_0 is a compactly supported L^2 function, presumably highly oscillatory. We notice that the initial data U_0 is not assumed to have a Wentzel–Kramers–Brillouin–Jeffreys (WKBJ) form.

We are looking for Gaussian-beam-based semi-classical solutions for the above initial value problem in the WKBJ form,

$$U(x,t) \approx A(x,t)\exp\left(\frac{\imath\tau(x,t)}{\hbar}\right). \tag{3}$$

According to the Gaussian beam theory [22,24,16], we solve the following ODE system to obtain ingredients for constructing Gaussian beams [11]:

$$\frac{dx}{dt} = H_p(x(t),p(t)), \quad x|_{t=0} = x_0, \tag{4}$$

$$\frac{dp}{dt} = -H_x(x(t),p(t)), \quad p|_{t=0} = p_0, \tag{5}$$

$$\frac{d\tau}{dt} = p(t)\cdot H_p(x(t),p(t)) - H(x(t),p(t)), \quad \tau|_{t=0} = x_0\cdot p_0, \tag{6}$$

$$\frac{dB}{dt} = -H_{xp}^T(x(t),p(t))B(t) - H_{xx}(x(t),p(t))C(t), \quad B|_{t=0} = \imath I, \tag{7}$$

$$\frac{dC}{dt} = H_{pp}(x(t),p(t))B(t) + H_{px}(x(t),p(t))C(t), \quad C|_{t=0} = I, \tag{8}$$

$$\frac{dA}{dt} = -\frac{1}{2}\mathrm{trace}(B(t)C^{-1}(t))A(t), \quad A|_{t=0} = A_0(x_0,p_0), \tag{9}$$

where the Hamiltonian $H(x,p) = \frac{1}{2}p^2 + V(x)$ is derived from the Schrödinger equation. Here $\{(x(t),p(t)):0\leqslant t\leqslant T\}$ defines a bicharacteristic emanating from the initial point (x_0,p_0), and the x-projection of this bicharacteristic defines a ray γ in the physical space, $\gamma = \{(x(t),t):0\leqslant t\leqslant T\}$. $\tau(t)$ is the phase function along the ray γ, and $A(t)$ is the amplitude function along the ray γ. $B(t)$ and $C(t)$ yield the Hessian of the phase function along γ: $B(t)C^{-1}(t) = \tau_{xx}(x(t),t)$; see [22,24] for the justification. See [11] for more details.

Moreover, the following lemmas hold [22,16,24]:

Lemma 2.1. *Under the above assumptions, $C(t)$ is non-singular for any t, and $\mathrm{Im}(BC^{-1})$ is positive definite.*

Lemma 2.2. *The solution for the transport equation (9) is*

$$A(t;x_0,p_0) = \frac{A_0(x_0,p_0)}{\sqrt{\det(C(t;x_0,p_0))}}. \tag{10}$$

According to the above ingredients, we define two globally smooth functions to approximate phase and amplitude functions required in the WKBJ ansatz,

$$\tau(x,t;x_0,p_0) = \tau(t;x_0,p_0) + p(t;x_0,p_0)\cdot(x - x(t;x_0,p_0)) + \frac{1}{2}(x - x(t;x_0,p_0))^T(BC^{-1})(x - x(t;x_0,p_0)), \tag{11}$$

$$A(x,t;x_0,p_0) = A(t;x_0,p_0). \tag{12}$$

Inserting (11) and (12) into the WKBJ ansatz yields an asymptotically valid solution:

$$\Psi(x,t;x_0,p_0) = A(x,t;x_0,p_0)\exp\left[\imath\frac{\tau(x,t;x_0,p_0)}{\hbar}\right]; \tag{13}$$

this is a single beam solution concentrated on the ray γ which is the x-projection of the bicharacteristic emanating from (x_0,p_0) at $t = 0$.

To justify that the beam solution constructed this way is a valid asymptotic solution for the initial value problem (1) and (2), we have to take into account the initial condition (2) in the beam construction. However, this depends upon how the initial condition is decomposed into Gaussian profiles and how the beam propagation is initialized; see [12,24,11,23,20,21] for several different approaches in terms of decomposing initial conditions into Gaussian profiles. In particular, in [11] the FBI transform has been first used to decompose the initial data into Gaussian profiles in the context of initializing beam propagation in both Lagrangian and Eulerian formulations.

2.2. The Fourier–Bros–Iagolnitzer (FBI) transform

Given $g\in L^2(\mathbb{R}^d)$, the Fourier–Bros–Iagolnitzer transform [15] is defined by the following formula:

$$\hat{g}(x,p;\hbar) = \mathcal{T}g(x,p;\hbar) = \alpha_{d,\hbar}\int_y \exp\left[\frac{\imath(x-y)\cdot p}{\hbar}\right]\exp\left[-\frac{(x-y)^2}{2\hbar}\right]g(y)dy, \tag{14}$$

with the normalization constant given by

$$\alpha_{d,\hbar} = 2^{-d/2}(\pi\hbar)^{-3d/4}, \tag{15}$$

where d is the dimensionality. Here the multiplication by the function $\exp\left[\frac{\imath x\cdot p}{\hbar}\right]$ in the FBI transform is done only for the convenience of having a convolution operator.

To demonstrate the behavior of this transformation, we consider the so-called *coherent state* $g(x) = \exp[-x^2/(2\hbar)]\exp\left(\imath\frac{p_0\cdot x}{\hbar}\right)$ which oscillates on the $O(\hbar)$ scale in a neighborhood of $x = 0$, where p_0 is a quantity of $O(1)$. A straight-forward calculation gives

$$\hat{g}(x,p;\hbar) = c\exp\left[\frac{\imath x\cdot p}{\hbar}\right]\exp\left[-\frac{x^2+(p-p_0)^2}{4\hbar}\right]\exp\left[-\frac{\imath x\cdot(p-p_0)}{2\hbar}\right]$$

for some normalization constant c; this implies that in this case the FBI coefficient divided by $\exp[\frac{\imath x\cdot p}{\hbar}]$ oscillates on the scale of $O(\hbar^{1/2})$ in both x- and p-directions. Moreover, according to [15, p. 96], all $u \in S'(\mathbb{R}^d)$ (the Schwartz space of tempered distributions on $\mathbb{R}^d$) can be written as a superposition of coherent states; consequently, we may assume that the FBI transform of the initial condition divided by $\exp\left[\frac{\imath x\cdot p}{\hbar}\right]$ ("the modified FBI coefficient"), $\widehat{U}_0(x,p;\hbar)\exp[-\frac{\imath x\cdot p}{\hbar}]$, oscillates on the scale of $O(\hbar^{1/2})$ in both x- and p-directions.

Another explanation for the definition of the FBI transform relies on the uncertainty principle. The transformation tries to have the errors $m(x)$ and $m(p)$ made in a measurement of the position and the momentum satisfy $m(x)\sim m(p)\sim\hbar^{1/2}$ by localizing g near x up to $O(\hbar^{1/2})$ by multiplying it with the Gaussian function $\exp[-(x-y)^2/2\hbar]$ and by localizing $\mathcal{F}_\hbar g$ near p up to $O(\hbar^{1/2})$ by taking the $\hbar$-Fourier transform with respect to y [15, p. 69]. We refer interested readers to [15] for more analysis of the FBI transform. Moreover, we also have the following identity [15]: $\|\mathcal{T}g\|_{L^2(\mathbb{R}^{2d})} = \|g\|_{L^2(\mathbb{R}^d)}$.

Thus according to [11], we first apply the FBI transform to the initial condition (2) to obtain $\widehat{U}_0(x,p;\hbar) = (\mathcal{T}U_0)(x,p;\hbar)$, and we then initialize the amplitude function in Eq. (9) by

$$A|_{t=0} = A_0(x_0,p_0) = \widehat{U}_0(x_0,p_0;\hbar)\exp\left[-\frac{\imath x_0\cdot p_0}{\hbar}\right]; \tag{16}$$

this way the amplitude A is initialized to be the *modified FBI* coefficient so that it oscillates on the scale of $O(\hbar^{1/2})$ in both x- and p-directions.

Based upon the above setup, the asymptotic solution to the Schrödinger equation is obtained by integrating all the beams parametrized by the initial point (x_0,p_0):

$$U(x,t) = \alpha_{d,\hbar}\int_{p_0}\int_{x_0}\Psi(x,t;x_0,p_0)dx_0dp_0. \tag{17}$$

As shown in [11], this beam solution satisfies the initial condition.

To specify initial data under consideration more precisely, we use the following definition of the *frequency set* of U_0 according to Martinez [15, p. 98].

Definition 2.3. A point $(x_0,p_0)\in\mathbb{R}^{2n}$ is not in the *frequency set* of an $\hbar$-dependent function $U_0\in L^2(\mathbb{R}^n)$ if and only if $\mathcal{T}U_0(x,p;\hbar) = O(\hbar^\infty)$ uniformly in a neighborhood of (x_0,p_0).

Therefore, in addition to U_0 being a compactly supported L^2-function and the modified FBI coefficient of U_0 oscillating on the scale of $O(\hbar^{1/2})$ in both x- and p-directions, we further assume that the *frequency set* of U_0 is compactly supported. This assumption is reasonable because the frequency set is defined in phase space rather than in frequency space and the FBI transform of U_0 can be *infinitely small rather than zero* in the complement of the frequency set of U_0. Thus, we conclude that for arbitrary $\eta > 0$ the set

$$\Omega_\eta = \{(x,p) : |\widehat{U}_0(x,p;\hbar)| > \eta\}$$

is bounded and measurable. Consequently, given $\eta > 0$, the global asymptotic solution to the Schrödinger equation is obtained by integrating all the beams parameterized by the initial point $(x_0,p_0)\in\Omega_\eta$,

$$U_\eta(x,t) = \alpha_{d,\hbar}\int_{(x_0,p_0)\in\Omega_\eta}\Psi(x,t;x_0,p_0)dx_0dp_0. \tag{18}$$

The FBI transform has been numerically implemented in [11]. To be complete, we summarize the implementation in [11] in the following. We denote $U_{0,i} = U_0(x_i)$ at the grid points x_i for $i = 1,\ldots,I$. Consider an equivalent form of the FBI transform,

$$\widehat{U}_0 = \mathcal{T}U_0 = \alpha_{d,\hbar}\int_y\exp\left[-\frac{(x-y)^2}{2\hbar}+\frac{p\cdot(x-y)\imath}{\hbar}\right]U_0(y)dy. \tag{19}$$

One way to determine $\widehat{U}(x_{i'},p_{j'};\hbar)$ is to approximate the above integral using the midpoint quadrature,

$$\widehat{U}_0(x_{i'},p_{j'};\hbar) = \alpha_{d,\hbar}\Delta x\sum_{j=1}^{I}\exp\left[-\frac{(x_{i'}-x_j)^2}{2\hbar}+\frac{p_{j'}\cdot(x_{i'}-x_j)\imath}{\hbar}\right]U_{0,j} \tag{20}$$

for each individual $(x_{i'},p_{j'})$. In MATLAB, we do not implement this in a point-by-point fashion. For a one-dimensional numerical FBI transform, we first construct two matrices A and B with each entry given by $-(x_{i'}-x_j)^2/2\hbar$ and

$i(x_{i'} - x_j)/\hbar$, respectively. These two matrices are independent of $p_{j'}$ and are stored separately from the integration routine. Then, for each $p_{j'}$ we construct the matrix $\exp(\mathsf{A} + p_{j'}\mathsf{B})$ and multiply it by the vector containing $U_0(x_{i'})$. This gives $\widehat{U}_0(x_{i'}, p_{j'}; \hbar)$ for all $i' = 1, \ldots, I$ for a fixed $p_{j'}$.

The above approximation converges to the exact solution as the mesh size $\Delta x \to 0$. However, in practice, we have to avoid the aliasing error as in the numerical Fourier transform. For simplicity, we consider the one-dimensional case where $U_0(y)$ is real. We first rewrite (14) into

$$\mathcal{T}U_0 = \alpha_{d,h} \exp\left(\frac{\imath x p}{\hbar}\right) \int_y \exp\left[-\frac{(x-y)^2}{2\hbar}\right] \exp\left[-\frac{\imath y p}{\hbar}\right] U_0(y)dy. \tag{21}$$

To well-sample the oscillations from $\exp\left(-\frac{\imath y p}{\hbar}\right)$, we require

$$\frac{|p|\Delta x}{\hbar} < \frac{\pi}{2}, \tag{22}$$

which implies $p \in (-\hbar\pi/2\Delta x, \hbar\pi/2\Delta x)$.

To improve the computational complexity, we also truncate the Gaussians in the kernel and limit the evaluation of the integral in a small neighborhood of each x. For instance, the exponential term $\exp\left[-(x_{i'} - x_j)^2/(2\hbar)\right]$ decays to zero when $|x_{i'} - x_j|$ is larger than approximately $3\hbar^{1/2}$. We will further address this in Section 3.4.

2.3. Eulerian Gaussian beams (EGB)

First we summarize the construction of Eulerian Gaussian beams as developed in [12,11]. Starting from the Hamiltonian system (4) and (5), the essential idea is first to develop a PDE formulation of the phase flow map:

$$\Phi(t) = \Phi_t : (x_0, p_0) \to (x(t), p(t));$$

this can be achieved by embedding the Hamiltonian system into the Liouville equations in phase space. Assuming that $\phi \in C^1(\mathbb{R}^{2d+1}, \mathbb{R}^d)$ and $\psi \in C^1(\mathbb{R}^{2d+1}, \mathbb{R}^d)$, we have the following Liouville equations [12,11],

$$\phi_t + H_p \cdot \phi_x - H_x \cdot \phi_p = 0, \quad \phi(x, p, 0) = x, \tag{23}$$

$$\psi_t + H_p \cdot \psi_x - H_x \cdot \psi_p = 0, \quad \psi(x, p, 0) = p. \tag{24}$$

To understand the relation between the mapping $(\phi(\cdot, \cdot, t), \psi(\cdot, \cdot, t))$ and the phase flow map $\Phi(t)$, we observe that since Eqs. (23) and (24) are homogeneous linear advection equations, the initial condition

$$(\phi(x, p, 0) = x, \psi(x, p, 0) = p)$$

of the mapping $(\phi(\cdot, \cdot, t), \psi(\cdot, \cdot, t))$ is advected along the bicharacteristic emanating from the initial point (x,p), and $(\phi(x,p,t), \psi(x,p,t))$ refers to the initial value of the mapping as stated in [12,11]:

$$(\phi(x, p, t) = \phi(x_0, p_0, 0) = x_0, \psi(x, p, t) = \psi(x_0, p_0, 0) = p_0),$$

where (x_0, p_0) and (x,p) are connected by a unique bicharacteristic through the phase flow map $\Phi(t)(x_0, p_0) = (x,p)$ or $(x_0, p_0) = \Phi^{-1}(t)(x,p)$. Therefore, $(\phi(\cdot, \cdot, t), \psi(\cdot, \cdot, t))$ encodes the initial value of the mapping (ϕ, ψ) in the following sense:

$$\phi(x, p, t) = \phi(\Phi^{-1}(t)(x, p), 0) = \phi(\Phi(-t)(x, p), 0),$$
$$\psi(x, p, t) = \psi(\Phi^{-1}(t)(x, p), 0) = \psi(\Phi(-t)(x, p), 0),$$

where $\Phi^{-1}(t)$ is the inverse of the phase flow map of $\Phi(t)$. Because of the reversibility of the Hamiltonian flow, we also have $\Phi^{-1}(t) = \Phi(-t)$. The semi-Lagrangian method for computing Eulerian Gaussian beam ingredients and carrying out beam summation as first proposed in [12] essentially relies on this property; see [12,11] for more details. The backward phase flow method that we are going to develop also hinges on this crucial invertibility of the phase flow map which we assume to hold.

Furthermore, as developed in [11] we have the following Liouville equation for the phase T, matrices B and C, and the amplitude A,

$$T_t + H_p \cdot T_x - H_x \cdot T_p = p \cdot H_p(x, p) - H(x, p), \quad T(x, p, 0) = x \cdot p, \tag{25}$$

$$B_t + H_p \cdot B_x - H_x \cdot B_p = -H_{xp}^T B - H_{xx} C, \quad B|_{t=0} = \imath I, \tag{26}$$

$$C_t + H_p \cdot C_x - H_x \cdot C_p = H_{pp} B + H_{px} C, \quad C|_{t=0} = I, \tag{27}$$

$$A_t + H_p \cdot A_x - H_x \cdot A_p = -\frac{1}{2}\mathrm{trace}(BC^{-1})A, \quad A|_{t=0} = \widehat{U}_0(x, p; \hbar) \exp\left[-\frac{\imath x \cdot p}{\hbar}\right]. \tag{28}$$

We remark that initializing $B|_{t=0} = \imath I$ effectively complexifies the Liouville equations for B and C at the matrix level because B and C are coupled to each other; such complexification at the matrix level for the Liouville equation has been first proposed in [12].

Once we have the above ingredients at our disposal, the Eulerian Gaussian beam solution is constructed by [11]

$$U(x,t) = \alpha_{d,\hbar} \int_{p'} \int_{x'} \Psi_{\text{Euler}}(x,t;x',p')dx'dp', \tag{29}$$

where

$$\Psi_{\text{Euler}}(x,t;x',p') = A(x',p',t)\exp\left[\imath\frac{1}{\hbar}\tau(x,t;x',p')\right], \tag{30}$$

$$\tau(x,t;x',p') = T(x',p',t) + p'\cdot(x-x') + \frac{1}{2}(x-x')^T(BC^{-1})(x-x'). \tag{31}$$

Here we have used the phase flow map to transform the beam summation formula (17) into (29); see [12,11] for more details.

2.4. Beam reinitialization

As time evolves, the width of a Gaussian beam will change according to the imaginary part of the Hessian of the phase function. To demonstrate this effect, we follow a similar analysis as in [20] and consider the evolution of a single beam under the potential $V(x) = -\frac{V_0^2}{2}x^2$ for some $V_0 > 0$. Solving the system for B and C, we have

$$\begin{aligned} B(t) &= V_0[c_1\exp(V_0t) - c_2\exp(-V_0t)],\\ C(t) &= c_1\exp(V_0t) + c_2\exp(-V_0t), \end{aligned} \tag{32}$$

with $c_1 = (1+\imath\epsilon/V_0)/2$ and $c_2 = (1-\imath\epsilon/V_0)/2$. This implies that the beam width is approximately proportional to

$$\exp(V_0t)\sqrt{\frac{\hbar\left[V_0^2(1+\exp(-2V_0t))^2 + \epsilon^2(1-\exp(-2V_0t))^2\right]}{4\epsilon V_0^2}} \tag{33}$$

which grows exponentially in t. An overly-extended Gaussian beam not only leads to large approximation errors in the Taylor expansions of phase and amplitude functions but also makes the final summation extremely expensive. Therefore, to compute long-time beam propagation beyond the log-time scale, we have to control the growth of beam width to some extent.

One remedy is to impose a mask function locally to each beam as in [22,24] such that the contribution of a given beam is zero if the location is too far away from the central beam location. However, this may degrade the accuracy of the beam solution for a fixed finite $\hbar$.

Another remedy is to reinitialize the whole process by re-decomposing the wave function into a summation of beams with a given initial beam width. This is unfortunately difficult for usual WKBJ-type decomposition methods which require explicit representations of phase and amplitude functions in that the wave function will no longer have the WKBJ form in the presence of caustics. However, in our current formulation based on the FBI transform, once we have obtained a wave function at a given time, we can simply re-apply the FBI transform to decompose the wave function at that time into a summation of beams with a fixed finite width; based upon this decomposition we reinitialize beam propagation; this process can be repeated.

We remark that the reinitialization idea was first proposed in [20] in the context of fast-wavepacket-transform-based Lagrangian beam methods for the Schrödinger equation; see also [21] in the context of fast-multiscale-wavepacket-transform-based Lagrangian Gaussian beam methods for the wave equation. Inspired by Qian and Ying [20,21], we use the idea in the context of FBI-transform-based Eulerian Gaussian beams for the Schrödinger equation. Numerically, one can monitor the width of each beam as it propagates. Once the width of a beam reaches a certain specified threshold, we can construct the overall wavefield and reinitialize the evolution. On the other hand, if the Hessian of the potential is known, one can have a rough estimate of the time period for reinitialization as explained in [20] and as demonstrated later in our examples.

We remark in passing that beam reinitialization may help to offset the effect of the errors in beam construction, which will make Gaussian beam valid for longer time. However, due to the inherent limitation of asymptotics which does not solve the PDE exactly, beam reinitialization will not offset the effect of asymptotic errors which builds up as time goes on.

3. The backward phase flow for FBI-based Eulerian beams

3.1. The algorithm

We are interested in developing a highly efficient Eulerian Gaussian beam framework to compute beam ingredients rapidly. Inspired by the original phase flow method [25], we propose the backward phase flow method to achieve this purpose.

The original phase flow method was developed in [25] in the context of obtaining geometrical optics approximation to the wave equation. The idea is to first construct the phase flow map for a fixed, small step size Δt and then apply it iteratively by virtue of the group property of the phase flow. For instance, one obtains the map from t_0 to t_1,

$$\Phi_{\Delta t} : (x_i, p_j; t_0) \to (x(t_1), p(t_1); t_1)$$

with $\Delta t = t_1 - t_0$. Thus, the value of the phase flow map (the arrival location of a bicharacteristic) at $t_2 = 2\Delta t$ with an initial condition $(x,p) = (x_i,p_j)$ can be computed by

$$\Phi_{\Delta t}(\Phi_{\Delta t}(x_i,p_j;t_0)) = \Phi_{\Delta t}\circ\Phi_{\Delta t}(x_i,p_j;t_0) = \Phi^2_{\Delta t}(x_i,p_j;t_0). \tag{34}$$

Indeed, the phase flow method is very efficient. One can obtain the solution for large t by first constructing the phase flow map for a small Δt (as an overhead) and then marching forward by interpolation since the phase flow map is defined on an invariant manifold [25]. Most of the computational overhead occurs during the pre-processing step. The interpolation can be done very rapidly. We refer interested readers to [25] for a complete description of the original algorithm.

To develop an Eulerian method for beam propagation, we will apply the phase flow method *backward* in time. We first construct the following backward phase flow map,

$$\Phi_{-\Delta t} : (x_i,p_j;t_1) \to (x(t_0),p(t_0);t_0),$$

which maps the point (x_i,p_j) at $t = t_1$ back to $t = t_0$ for some $\Delta t = t_1 - t_0$. To determine the take-off location of a bicharacteristic reaching the point (x_i,p_j) at $t = t_k = k\Delta\, t$, we iterate this backward phase flow map and get $\Phi^k_{-\Delta t}(x_i,p_j;t_k)$.

On the other hand, this approach is also similar to the semi-Lagrangian method. For example, both of these approaches compute solutions on a fixed mesh by tracing trajectories backward in time. In the typical semi-Lagrangian method, on the other hand, one traces the solution backward in time from $t = t^{n+1}$ for one time step Δt and then one interpolates the function value at $t = t^n$ right away. In the *global* semi-Lagrangian method that we have used [13,12,11], one traces the solutions all the way back from $t = t^{n+1}$ to $t = t^0$ to avoid interpolations in the solutions. The current proposed approach can be interpreted as a generalization of these semi-Lagrangian methods, which on one hand speeds up the *global* semi-Lagrangian method and on the other hand reduces the number of interpolations.

However, for the phase equation

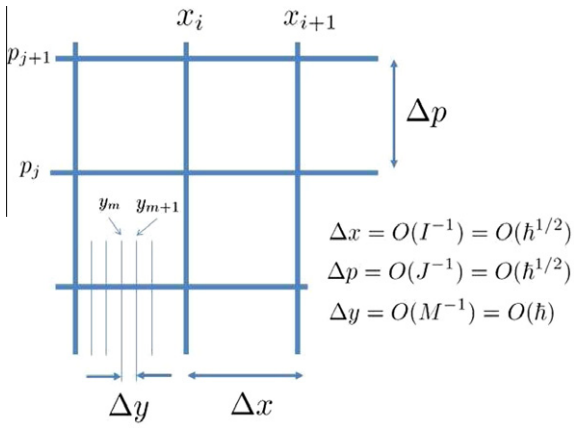

Fig. 1. Discretization of phase space.

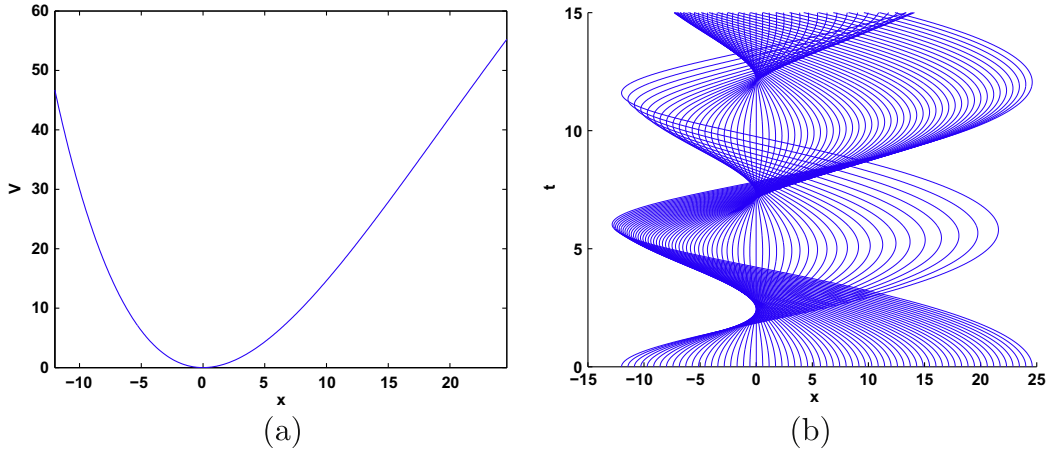

Fig. 2. (Example 5.1) (a) The Morse potential and (b) the ray structure up to time $t = 15$.

$$\frac{DT}{Dt} = p \cdot H_p(x,p) - H(x,p), \tag{35}$$

where D/Dt is the material derivative defined by

$$\frac{D}{Dt} = \frac{\partial}{\partial t} + H_p \frac{\partial}{\partial x} - H_x \frac{\partial}{\partial p},$$

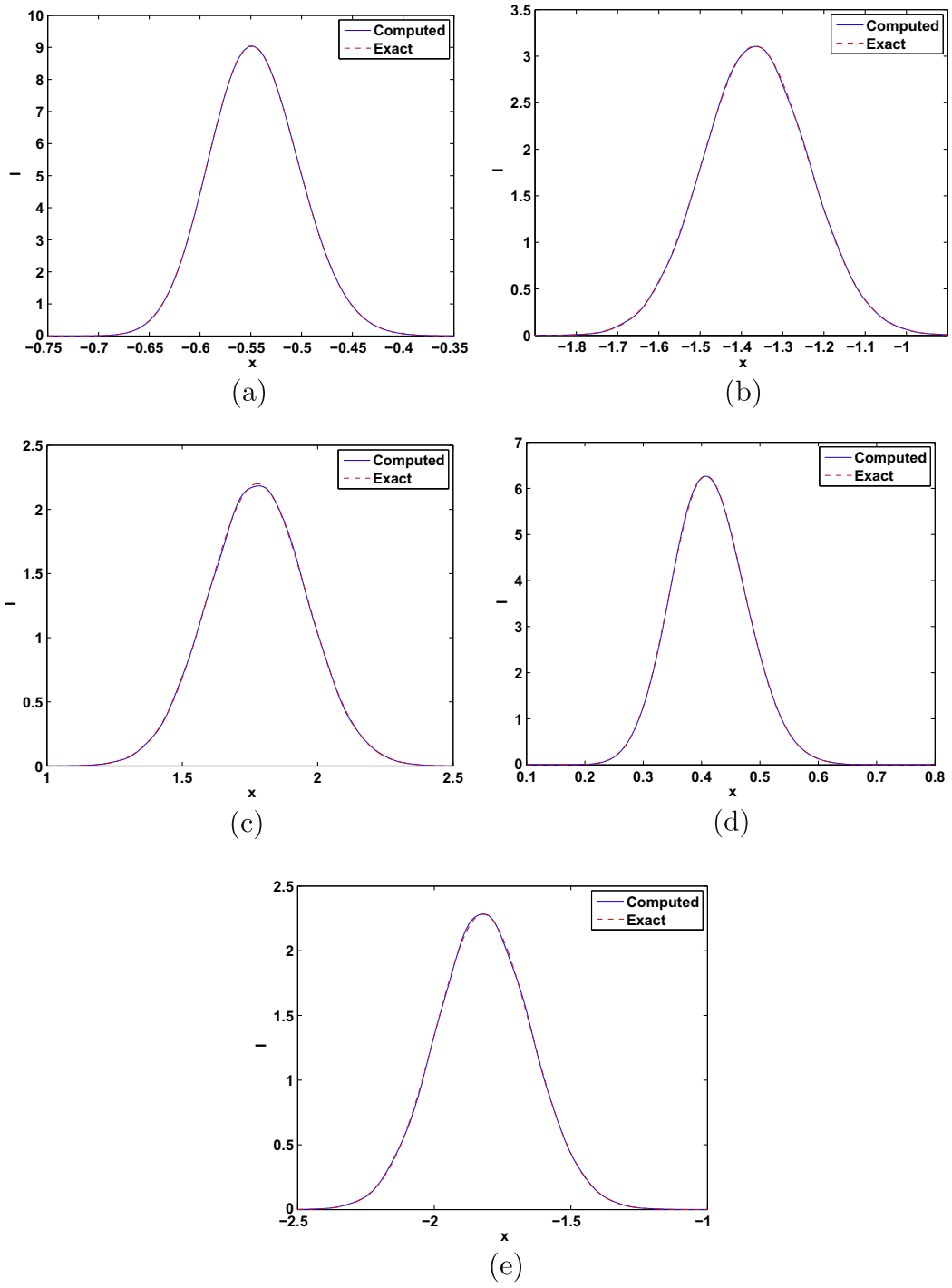

Fig. 3. (Example 5.1) $h = 1/32$ and the phase flow map step size $\Delta t = 1.5$. Eulerian Gaussian beam summations with beam reinitialization using the backward phase flow method on a mesh $I = J = 256$, $M = 2^{11} + 1$. The position densities at (a) $t = 2\Delta\, t = 3$, (b) $t = 4\Delta t = 6$, (c) $t = 6\Delta t = 9$, (d) $t = 8\Delta\, t = 12$ and (e) $t = 10\Delta t = 15$.

we cannot directly apply the above procedure to obtain the phase information at a later time since the method applies only to the bicharacteristic variables. To solve this reaction equation along the bicharacteristic based on the backward phase flow map, we use the fact that this ODE is autonomous; therefore, if we denote $T_{-\Delta t}(x_i,p_j;t_1)$ the backward map given by the bicharacteristic reaching (x_i,p_j) at $t=t_1$ starting from $(x(t_0),p(t_0))$, the solution at $(x_i,p_j;t_k)$ can be computed by

$$T(x_i,p_j;t_k)=x(t_0)\cdot p(t_0)+\sum_{n=0}^{k-1} T_{-\Delta t}(\Phi^n_{-\Delta t}(x_i,p_j);t_{k-n}), \tag{36}$$

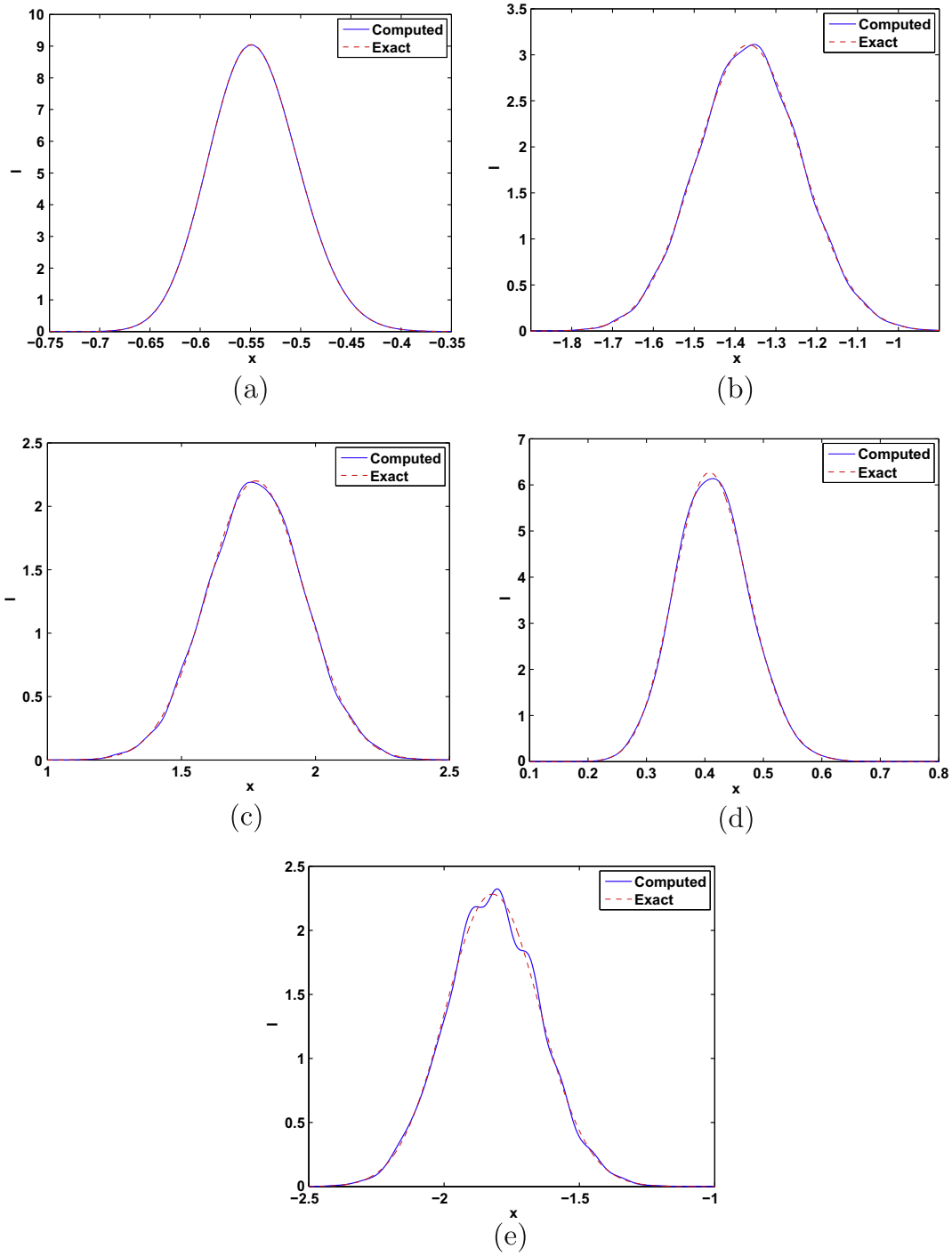

Fig. 4. (Example 5.1) $h=1/32$ and the phase flow map step size $\Delta t=3.0$. Eulerian Gaussian beam summations with beam reinitialization using the backward phase flow method on a mesh $I=J=256$, $M=2^{11}+1$. The position densities at (a) $t=\Delta t=3$, (b) $t=2\Delta t=6$, (c) $t=3\Delta t=9$, (d) $t=4\Delta t=12$ and (e) $t=5\Delta t=15$.

where $\Phi^0_{-\Delta t}(x_i, p_j) = (x_i, p_j)$. Numerically, it is more natural to express the solution in the following iterative form:

$$T(x_i, p_j; t_k) = T_{-\Delta t}(x_i, p_j; t_k) + T(\Phi_{-\Delta t}(x_i, p_j); t_{k-1}). \tag{37}$$

With beam reinitialization, one resets the phase variable in the FBI transform. This implies that we can simply construct the map $T_{-\Delta t}(x_i, p_j)$, which is independent of t_{k-1}, and then assign

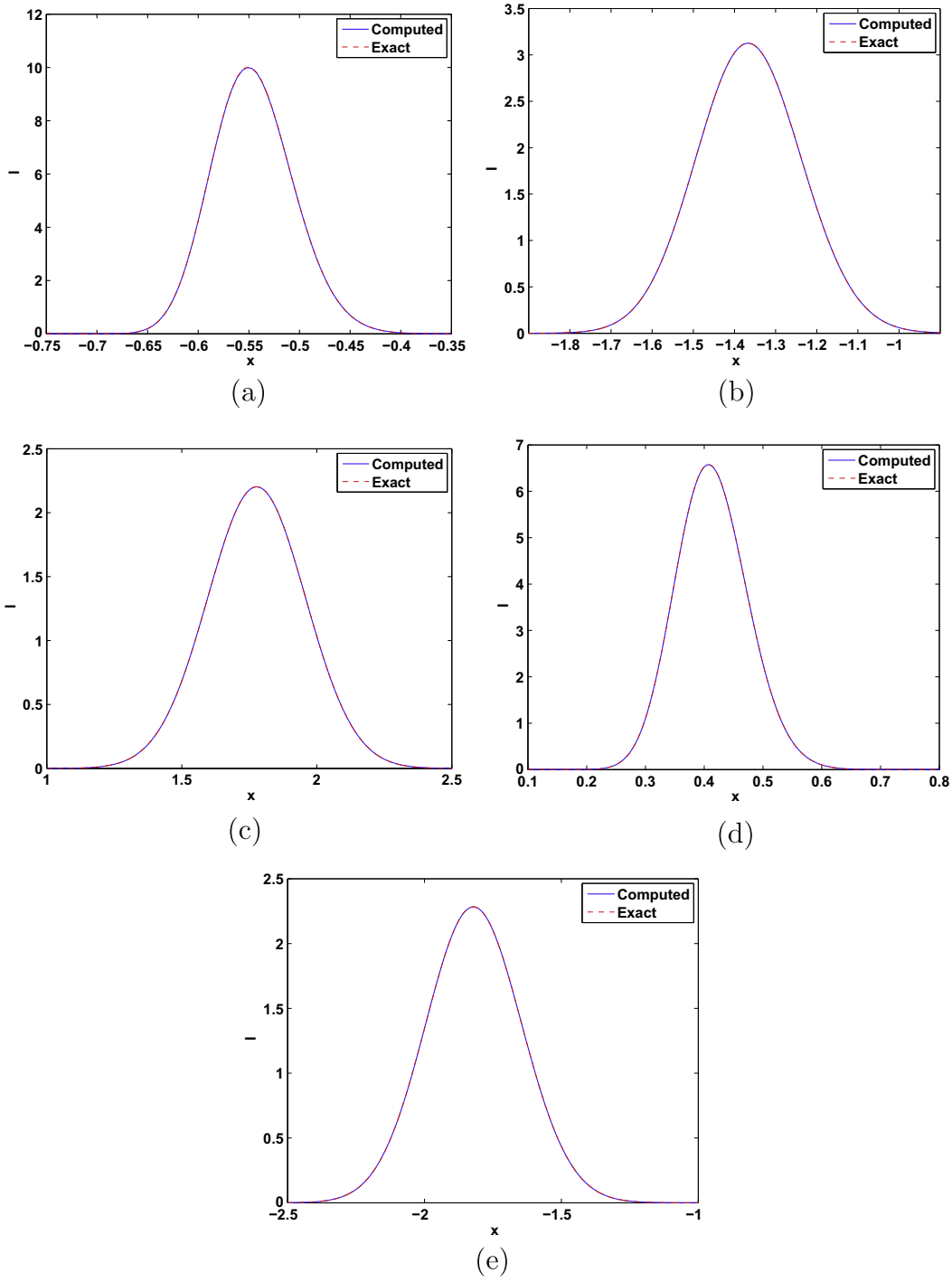

Fig. 5. (Example 5.1) $\hbar = 1/128$ and the phase flow map step size $\Delta t = 1.5$. Eulerian Gaussian beam summations with beam reinitialization using the backward phase flow method on a mesh $I = J = 1025$, $M = 2^{11} + 1$. The position densities at (a) $t = 2\Delta\ t = 3$, (b) $t = 4\Delta t = 6$, (c) $t = 6\Delta t = 9$, (d) $t = 8\Delta\ t = 12$ and (e) $t = 10\Delta t = 15$.

$$T(x_i, p_j; t_k) = T_{-\Delta t}(x_i, p_j) + \tilde{x}_i \cdot \tilde{p}_j \tag{38}$$

where $(\tilde{x}_i, \tilde{p}_j) = \Phi_{-\Delta t}(x_i, p_j)$.

We follow a similar idea for solving B and C. We first obtain the following maps $B_{-\Delta t}(x_i, p_j)$ and $C_{-\Delta t}(x_i, p_j)$ which correspond to the solution to

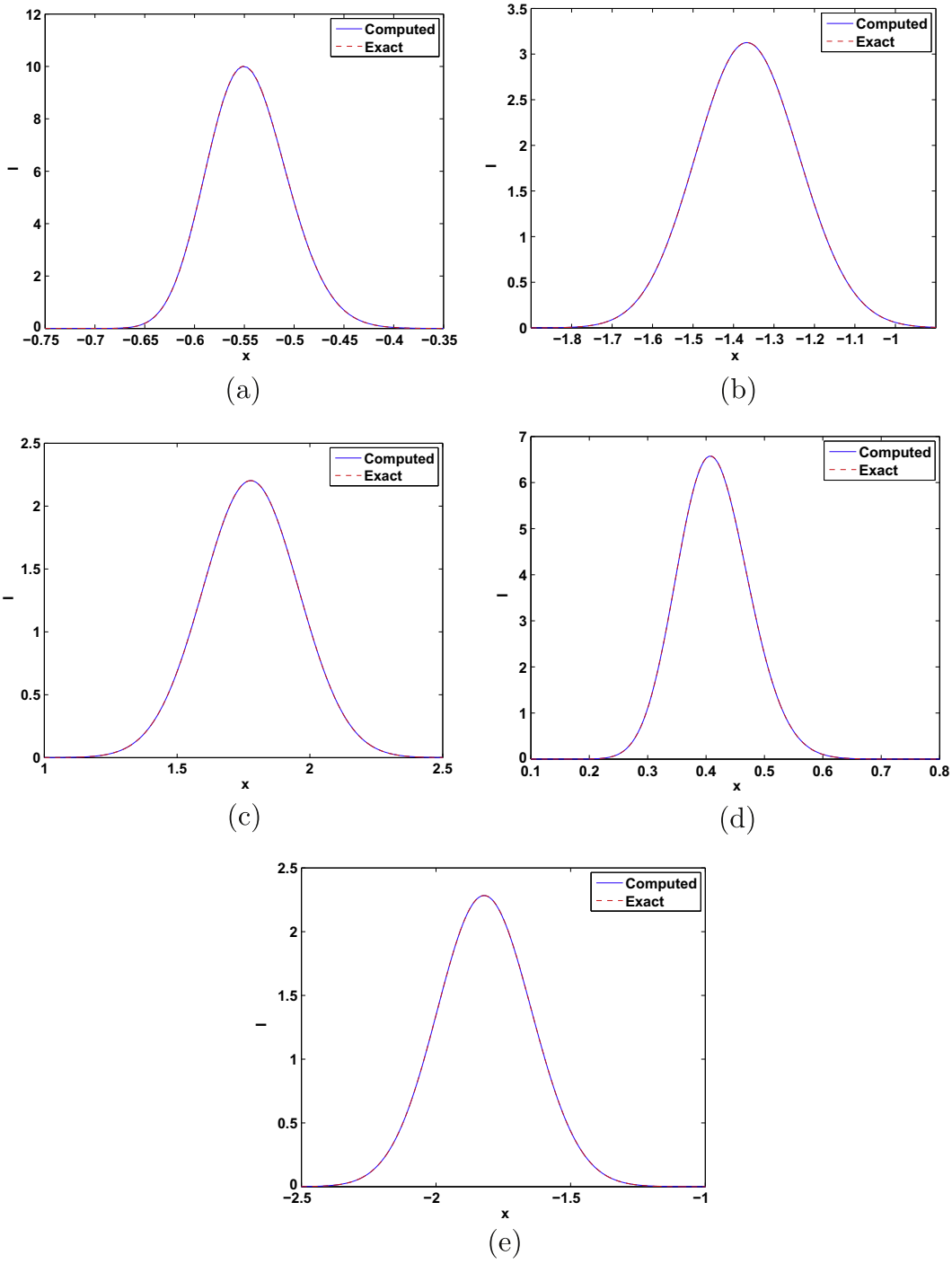

Fig. 6. (Example 5.1) $h = 1/128$ and the phase flow map step size $\Delta t = 3.0$. Eulerian Gaussian beam summations with beam reinitialization using the backward phase flow method on a mesh $I = J = 1025$, $M = 2^{11} + 1$. The position densities at (a) $t = \Delta t = 3$, (b) $t = 2\Delta t = 6$, (c) $t = 3\Delta t = 9$, (d) $t = 4\Delta t = 12$ and (e) $t = 5\Delta t = 15$.

$$\begin{aligned}\frac{DB}{Dt} &= -H_{xp}^T B - H_{xx} C,\\ \frac{DC}{Dt} &= H_{pp}^T B + H_{px} C,\end{aligned} \tag{39}$$

along the bicharacteristic with the initial conditions $B(x,p) = \imath I$ and $C(x,p) = I$. With beam reinitialization in phase space using the FBI transform, we simply have

$$\begin{aligned}B(x_i,p_j;t_k) &= B_{-\Delta t}(x_i,p_j),\\ C(x_i,p_j;t_k) &= C_{-\Delta t}(x_i,p_j).\end{aligned} \tag{40}$$

Next, we consider the amplitude function A. This function satisfies the transport equation

$$\frac{DA}{Dt} = -\frac{1}{2}\mathrm{trace}(BC^{-1})A \tag{41}$$

along the bicharacteristic arriving at $(x_i,p_j;t_1)$ from the initial point at $(x(t_0),p(t_0))$. This ODE is different from the equation for the phase since we do not have the reciprocal principle. To obtain the solution based on the backward phase flow map, we first obtain the following map $A_{-\Delta t} : (x_i,p_j) \to \mathbb{C}$ which maps the location (x_i,p_j) at $t = t_1$ to the solution to the above ODE with the initial condition given by $A(x(t_0),p(t_0)) = 1$. Using the analytical solution to the transport equation (10), we have

$$A(x_i,p_j;t_1) = A_{-\Delta t}(x_i,p_j)A_0(\Phi_{-\Delta t}(x_i,p_j)), \tag{42}$$

where $A_0(\Phi_{-\Delta t}(x_i,p_j))$ is the modified FBI coefficient at the takeoff location $\Phi_{-\Delta t}(x_i,p_j)$. To obtain the solution at $t = t_2$, we iterate the map one more time and get

$$A(x_i,p_j;t_2) = A_{-\Delta t}(x_i,p_j)A(\Phi_{-\Delta t}(x_i,p_j);t_1) = A_{-\Delta t}(x_i,p_j)A_{-\Delta t}(\Phi_{-\Delta t}(x_i,p_j))A_0(\Phi^2_{-\Delta t}(x_i,p_j)). \tag{43}$$

In general we have the following relation to link $A(x_i,p_j;t_n)$ to the initial condition $A_0(x,p)$ through

$$A(x_i,p_j;t_k) = \left[\prod_{n=0}^{k-1} A_{-\Delta t}\left(\Phi^n_{-\Delta t}(x_i,p_j)\right)\right] A_0\left(\Phi^k_{-\Delta t}(x_i,p_j)\right). \tag{44}$$

However, since we reinitialize beam propagation in phase space using the FBI transform, we can simply use

$$A(x_i,p_j;t_k) = A_{-\Delta t}(x_i,p_j)A_{k-1}(\Phi_{-\Delta t}(x_i,p_j)), \tag{45}$$

where $A_{k-1}(x,p)$ is the reinitialized amplitude function at $t = t_{k-1}$.

We summarize the above ingredients into an algorithm. To be specific, we outline the algorithm for the one-dimensional case only.

Algorithm: EGB-backward phase flow with beam reinitialization ($d = 1$)

1. Discretize the computational domain

$$\begin{aligned}x_i &= x_{\min} + (i-1)\Delta x, \quad \Delta x = \frac{x_{\max}-x_{\min}}{I-1}, \quad i = 1,2,\ldots,I\\ p_j &= p_{\min} + (j-1)\Delta p, \quad \Delta p = \frac{p_{\max}-p_{\min}}{J-1}, \quad j = 1,2,\ldots,J\\ y_m &= x_{\min} + (m-1)\Delta y, \quad \Delta y = \frac{x_{\max}-x_{\min}}{M-1}, \quad m = 1,2,\ldots,M\\ t_k &= t_0 + k\Delta t, \quad \Delta t = \frac{t_f - t_0}{K}, \quad k = 1,2,\ldots,K.\end{aligned}$$

2. Construct the phase flow map and other maps

$$\Phi_{-\Delta t}(x_i,p_j), T_{-\Delta t}(x_i,p_j), A_{-\Delta t}(x_i,p_j), B_{-\Delta t}(x_i,p_j) \quad \text{and} \quad C_{-\Delta t}(x_i,p_j).$$

3. Initialize $T(x_i,p_j;t_0) = x_i \cdot p_j$ and $A(x_i,p_j;t_0) = A_0(x_i,p_j)$.
4. For $k = 1,2,\ldots,K$, construct the solution at $t = t_k$,
   (a) $T(x_i,p_j;t_k) = T_{-\Delta t}(x_i,p_j) + \tilde{x}_i \cdot \tilde{p}_j$;
   (b) $A(x_i,p_j;t_k) = A_{k-1}(\Phi_{-\Delta t}(x_i,p_j))A_{-\Delta t}(x_i,p_j)$;
   (c) $B(x_i,p_j;t_k) = B_{-\Delta t}(x_i,p_j)$;
   (d) $C(x_i,p_j;t_k) = C_{-\Delta t}(x_i,p_j)$;
   (e) construct the wave function $U(y_i;t_k)$.

The extra set of mesh y_m in the above algorithm is used only in 4(e) for the purpose of visualization. More details in choosing M will be further discussed in Section 3.3. Numerically the most expensive step is to update the amplitude function

$A(x_i, p_j; t_k)$ in Step 4(b). Since the function A is in general highly oscillatory, usual interpolation methods generate significant errors which will degrade the accuracy of beam propagation. Therefore, we propose the following two different ways to obtain the quantity $A_{k-1}(\Phi_{-\Delta t}(x_i, p_j))$.

In the first approach, we consider not the overall wavefield but each beam individually. Since we have already obtained all individual beam solutions at $t = t_{k-1}$ arriving at phase space locations (x_i, p_j), we apply the FBI transform to each arrival beam to obtain $A_{k-1}(\Phi_{-\Delta t}(x_i, p_j))$. The second approach uses the overall wavefield not at the coarse mesh x_i but at the fine mesh y_m to accurately recover the phase information which is lost in the beam summation process.

3.2. Applying the FBI transform to each arrival beam

The first approach is to apply the FBI transform to each arrival beam at t_{k-1} and evaluate the amplitude function at $\Phi_{-\Delta t}(x_i, p_j)$. To do that, we assume that we have already obtained the wave function $\Psi_{i',j'} = \Psi(x, t_{k-1}; x_{i'}, p_{j'})$ contributed by the beam arriving at the grid location $(x, p) = (x_{i'}, p_{j'})$ at time $t = t_{k-1}$, where

$$\Psi_{i',j'} = \Psi(x, t_{k-1}; x_{i'}, p_{j'}) = A(x_{i'}, p_{j'}) \exp\left(\frac{\imath\tau(x, t_{k-1}; x_{i'}, p_{j'})}{\hbar}\right), \tag{46}$$

and

$$\tau(x, t_{k-1}; x_{i'}, p_{j'}) = T(x_{i'}, p_{j'}; t_{k-1}) + p_{j'}(x - x_{i'}) + \frac{1}{2}(x - x_{i'})^T (B(x_{i'}, p_{j'}; t_{k-1}) C(x_{i'}, p_{j'}; t_{k-1})^{-1})(x - x_{i'}). \tag{47}$$

Since beam summation consists of a finite number of terms and the FBI transform is linear, $A_{k-1}(\Phi_{-\Delta t}(x_i, p_j))$ can be computed by

$$A_{k-1}(\Phi_{-\Delta t}(x_i, p_j)) = \left(\sum_{i',j'} \mathcal{T}\Psi_{i',j'}\big|_{\Phi_{-\Delta t}(x_i,p_j)}\right) \exp\left[-\frac{\imath x' \cdot p'}{\hbar}\right], \tag{48}$$

where $\mathcal{T}$ is the FBI transform operator, and $\Phi_{-\Delta t}(x_i, p_j) = (x', p')$. For the arrival beam $\Psi_{i',j'}$, we can estimate the local neighborhood of $(x_{i'}, p_{j'})$ such that $|\mathcal{T}\Psi_{i',j'}| \neq 0$. For instance, applying the FBI transform to the above Gaussian beam, we obtain the following estimate analytically,

$$|\mathcal{T}\Psi_{i',j'}|^2 = O\left(\exp\left[-\frac{1}{2}\begin{pmatrix} x - x_{i'} \\ p - p_{j'} \end{pmatrix}^T \overline{M} \begin{pmatrix} x - x_{i'} \\ p - p_{j'} \end{pmatrix}\right]\right), \tag{49}$$

where the covariance matrix $\overline{M}$ is given by

$$\overline{M} = \frac{2}{\hbar(\beta_1^2 + \beta_2^2)} \begin{pmatrix} \beta_1^2 - \beta_1 + \beta_2, & -\beta_2 \\ -\beta_2, & \beta_1 \end{pmatrix} \tag{50}$$

with

$$\begin{aligned} \beta_1 &= 1 + \mathrm{Im}\left(B(x_{i'}, p_{j'}; t_{k-1}) C(x_{i'}, p_{j'}; t_{k-1})^{-1}\right), \\ \beta_2 &= \mathrm{Re}\left(B(x_{i'}, p_{j'}; t_{k-1}) C(x_{i'}, p_{j'}; t_{k-1})^{-1}\right). \end{aligned} \tag{51}$$

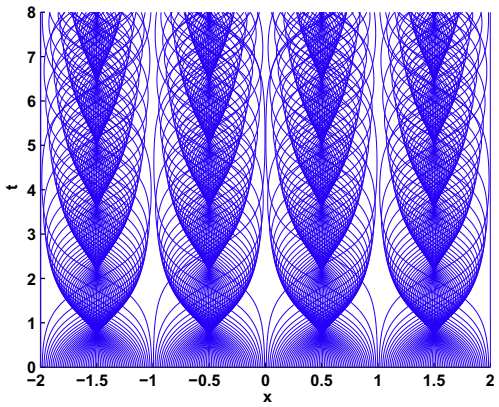

Fig. 7. (Example 5.2) The complicated ray structure up to time $t = 8$.

This implies that the magnitude of $\mathcal{T}\Psi_{i',j'}$ decays exponentially in the directions of the eigenvectors of $\overline{M}$ with standard deviations related to their corresponding eigenvalues. Therefore, all numerical FBI transforms can be computed locally in the small neighborhood of the beam arrival location $(x_{i'}, p_{j'})$.

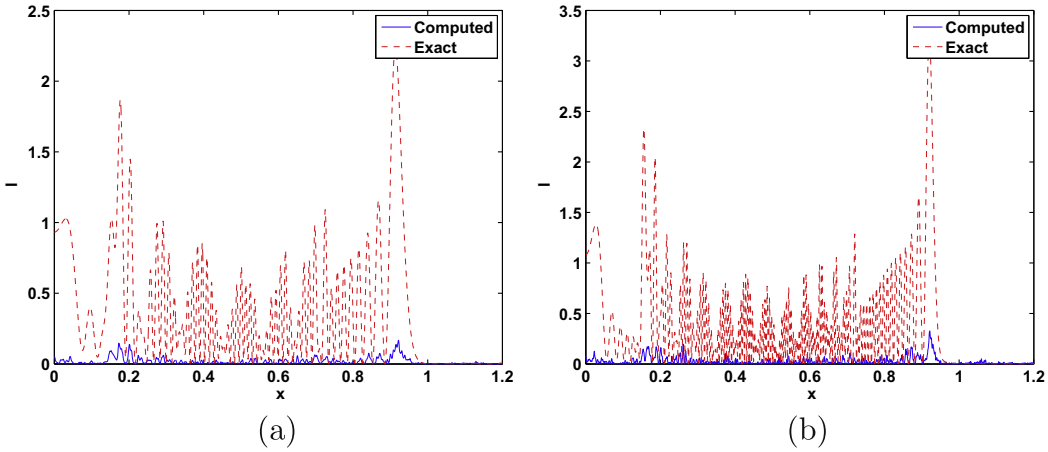

Fig. 8. (Example 5.2) Eulerian Gaussian beam summations without beam reinitialization using the backward phase flow method on a mesh $I = J = 256$, $M = 2^{14} + 1$. The position densities at $t = 8$ with (a) $h = 1/64$ and (b) $h = 1/128$.

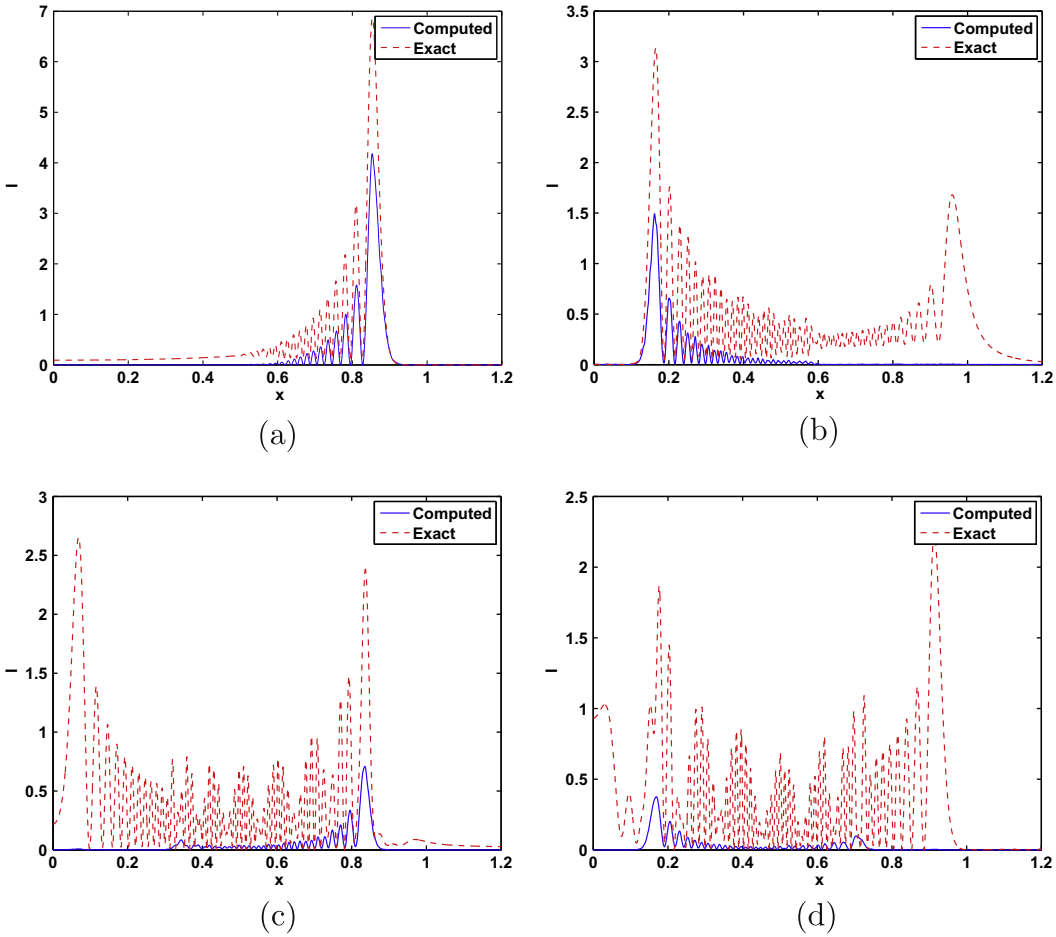

Fig. 9. (Example 5.2) $h = 1/64$ and the phase flow map step size $\Delta t = 2.0$. Eulerian Gaussian beam summations with beam reinitialization using the backward phase flow method on a mesh $I = J = 256$, $M = 2^{14} + 1$. The position densities at (a) $t = \Delta\ t = 2$, (b) $t = 2\Delta t = 4$, (c) $t = 3\Delta t = 6$, and (d) $t = 4\Delta\ t = 8$.

3.3. Applying the FBI transform to the overall wavefield

Indeed, the easiest way is to apply the FBI transform to the overall wavefield at $t = t_{k-1}$ and evaluate it at $\Phi_{-\Delta t}(x_i, p_j)$. One difficulty is that during the beam summation process, we have already lost the phase information in the overall wavefield. The FBI transform of the wavefield might introduce aliasing errors. In this section, we propose to first construct the overall wavefield defined on a fine mesh $y = y_m$ so that we can correctly capture the phase in the solution. As discussed in obtaining formula (22), for a fixed uniform sampling of the wavefield with a given Δy, referring to Fig. 1, one requires a certain bound on the range of p. In practice, if we use only the overall wavefield to compute the FBI coefficient, this restriction cannot be guaranteed in general.

One nice property of the current formulation is that the wavefield can be evaluated at *arbitrary* locations for a given set of arrival beams in phase space. Using the notation above, once we have obtained a set of beams at $t = t_k$ with non-zero $|A(x_i, p_j; t_k)|$, we check the range of p_j and compute

$$\bar{p}_j = \max\{|p_j| : \quad \text{for } i,j \ \{\text{such that } |A(x_i, p_j; t_k)| > \eta\},$$

where η is a prescribed positive constant. From the calculation in Eq. (49), the application of the FBI transform to an arrival beam will propagate information to a local region. We extend the range of p_j by $O(\hbar^{-1/2})$ and define a new range for p_j by

$$\mathcal{R}_k = [-\bar{p}_j - O(\hbar^{-1/2}), \bar{p}_j + O(\hbar^{-1/2})].$$

Then the number of sampling points, M, is chosen so that this range $\mathcal{R}_k$ lies inside the constraint from formula (22), $(-\hbar\pi/2\Delta y, \hbar\pi/2\Delta y)$. By over-sampling in the spatial domain, the FBI transform will not introduce aliasing errors, and we do not need to introduce any artificial mask in the transformation.

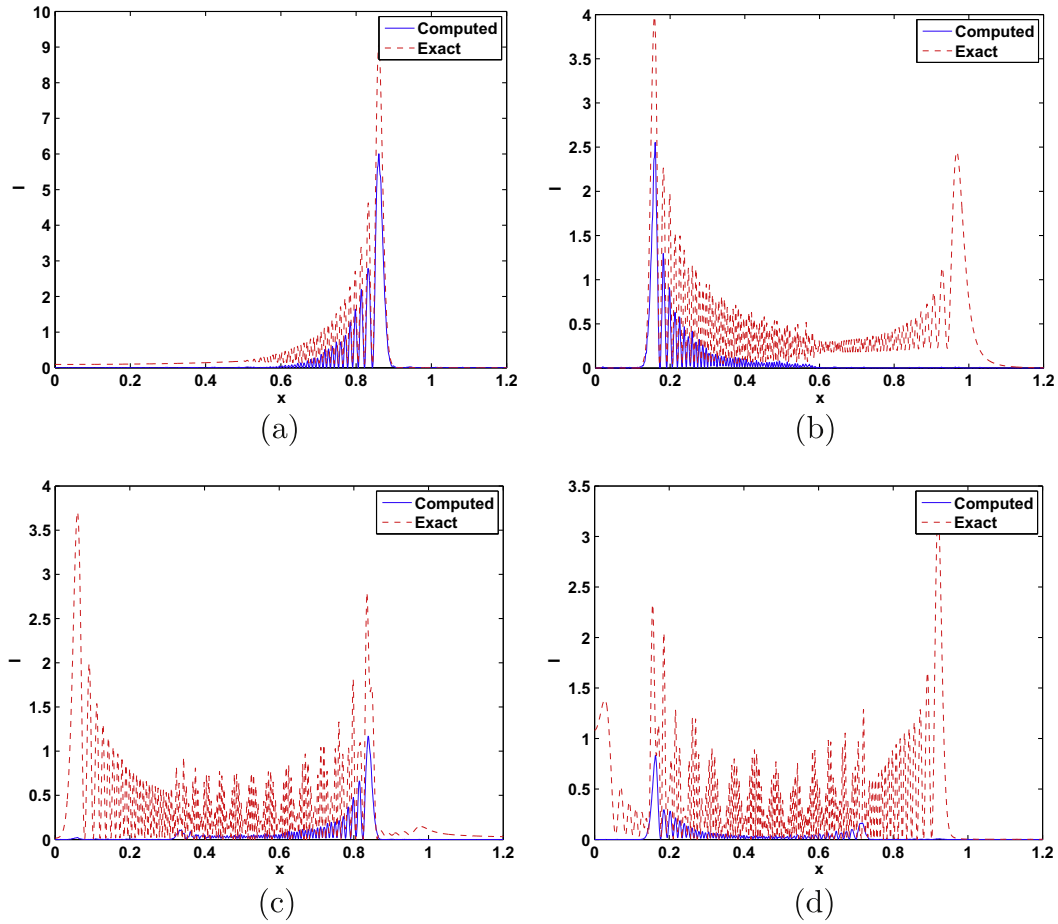

Fig. 10. (Example 5.2) $\hbar = 1/128$ and the phase flow map step size $\Delta t = 2.0$. Eulerian Gaussian beam summations with beam reinitialization using the backward phase flow method on a mesh $I = J = 256$, $M = 2^{14} + 1$. The position densities at (a) $t = \Delta\ t = 2$, (b) $t = 2\Delta t = 4$, (c) $t = 3\Delta t = 6$, and (d) $t = 4\Delta\ t = 8$.

3.4. Computational complexity

We first state the following orders of computational complexity in the above algorithm and then we will further discuss these estimates.

Computational complexity: EGB-backward phase flow with reinitialization ($d = 1$)

1. $I + J + M$.
2. IJN, with N the number of intermediate time steps to advance from t_0 to t_1.
3. $\alpha(I,J,M)$, the computational complexity of the numerical FBI transform on a mesh of $O(IJ)$ given $O(M)$ data.
4.
   (a) IJ;
   (b) $IJ + \alpha(I,J,M)$;
   (c) IJ;
   (d) IJ;
   (e) $\beta(I,J,M)$, the computational complexity of reconstructing the overall wavefield at $O(M)$ locations given FBI coefficients on a mesh of $O(IJ)$.

Since Step 4 will be iterated for K times, the overall computational complexity is of order

$$O(IJN + \alpha(I,J,M) + K[IJ + \alpha(I,J,M) + \beta(I,J,M)]) = O(IJ(K+N) + K[\alpha(I,J,M) + \beta(I,J,M)]). \quad (52)$$

Before we determine $\alpha(I,J,M)$ and $\beta(I,J,M)$, we first estimate I, J and M according to $\hbar$. For each $x_{i'}$, the exponential term $\exp\left[-(x_{i'} - x_j)^2/(2\hbar)\right]$ in the FBI transform decays to zero when $|x_{i'} - x_j|$ is larger than approximately $3\hbar^{1/2}$. To accurately resolve this Gaussian in the x-direction, we require $\Delta x = O(\hbar^{1/2})$ and so $I = O(\hbar^{-1/2})$. Next, for a given $x_{i'}$ and along the

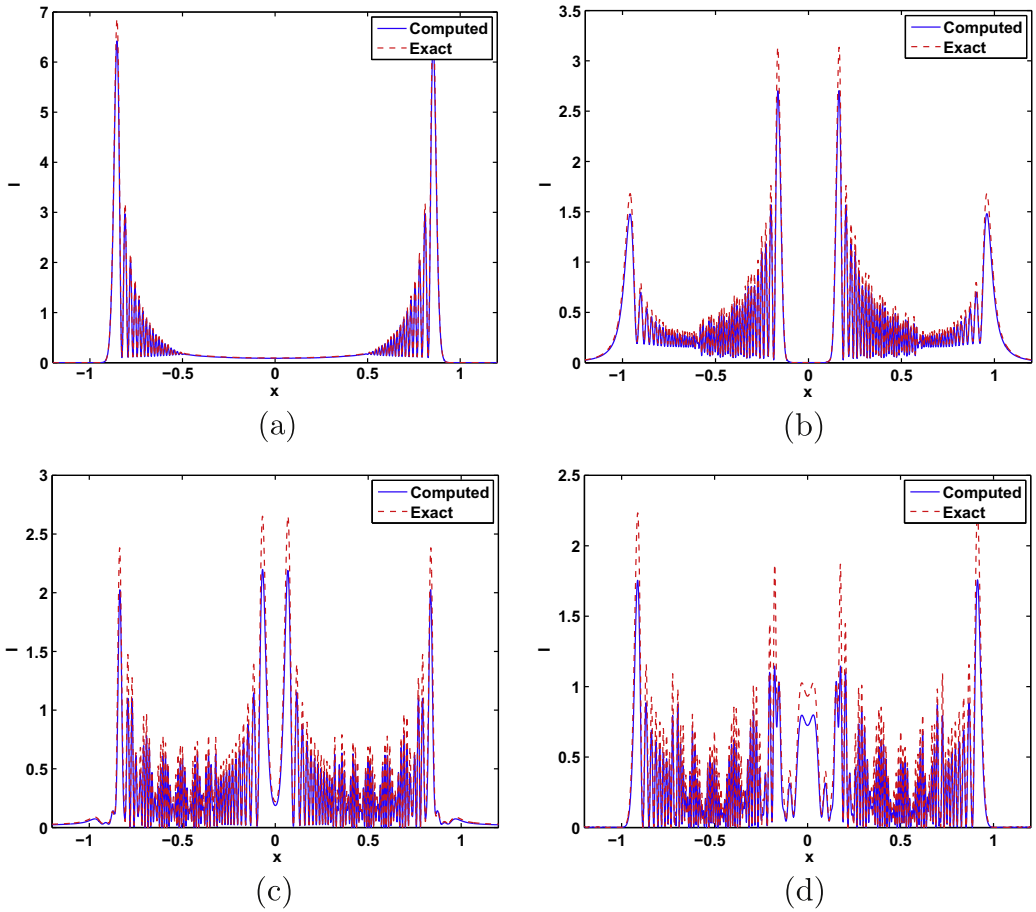

Fig. 11. (Example 5.2) $h = 1/64$ and the phase flow map step size $\Delta t = 0.40$. Eulerian Gaussian beam summations with beam reinitialization using the backward phase flow method on a mesh $I = J = 256$, $M = 2^{14} + 1$. The position densities at (a) $t = 5\Delta$ $t = 2$, (b) $t = 10\Delta t = 4$, (c) $t = 15\Delta t = 6$, and (d) $t = 20$ $\Delta t = 8$.

p-direction, the magnitude of the FBI coefficient is a Gaussian with the standard deviation $O(\hbar^{1/2})$, as seen in Eq. (49). To accurately resolve this Gaussian in the p-direction, we require $\Delta p = O(\hbar^{1/2})$ and so $J = O(\hbar^{-1/2})$. Concerning M, we require that Δy well-sample the oscillation in the FBI transform. According to Eq. (22) we have $\Delta y = O(\hbar)$ and $M = O(\hbar^{-1})$.

Next we consider the expressions $\alpha(I,J,M)$ and $\beta(I,J,M)$ related to the FBI transform and the number of Eulerian beams. At the first glance, it seems that we are required to sum up M terms for each grid point of the $I \times J$ grid in the FBI transform, which gives $O(IJM) = O(\hbar^{-2})$; however, this actually over-estimates the complexity because it does not take into account the decaying property of the Gaussian in the FBI transform. To compute each non-zero FBI coefficient, instead of summing up $O(M)$ terms in the FBI transform, one only needs to look at a local neighborhood with size of $O(\Delta x) = O(\hbar^{1/2})$. This means the computational cost for computing the FBI integral is $O(M/I) = O(\hbar^{-1/2})$. Moreover, since for a given $x_{i'}$, the FBI coefficient in the p-direction decays to zero in only few grid points, the total number of non-zero FBI coefficients is $O(I)$. This gives $\alpha(I,J,M)$ = the total number of non-zero FBI coefficients $\times$ computational complexity for computing each non-zero FBI coefficient = $O(I \cdot (M/I)) = O(\hbar^{-1})$.

Now we consider the expression $\beta(I,J,M)$, the computational complexity of the adjoint of the FBI transform; this is used to construct the overall wavefield on an $O(M)$ mesh using FBI coefficients on the $O(IJ)$ mesh. Since the computations of B and C are independent of $\hbar$, each beam contributes to a local neighborhood in the x-direction of size $O(\hbar^{-1/2})$. Since $\Delta y = O(\hbar)$ and we have only $O(I)$ non-zero Eulerian beams, we have $\beta(I,J,M)$ = the total number of arrival beams $\times$ computational complexity for computing the wavefield due to one beam = $O(I \cdot (M/I)) = O(\hbar^{-1})$.

In terms of $\hbar$, the overall computational complexity of the whole algorithm for one dimension ($d = 1$) is therefore

$$O(IJ(K+N) + K[\alpha(I,J,M) + \beta(I,J,M)]) = O(\hbar^{-1}(K+N)) = O(\hbar^{-1}). \tag{53}$$

We can develop similar algorithms for the d-dimensional case. The only modification in the above algorithm is that x_i, p_j, and y_m now become mesh points in $\mathbb{R}^d$. The derivation in Section 3.1 does not depend on the dimensionality of the domain.

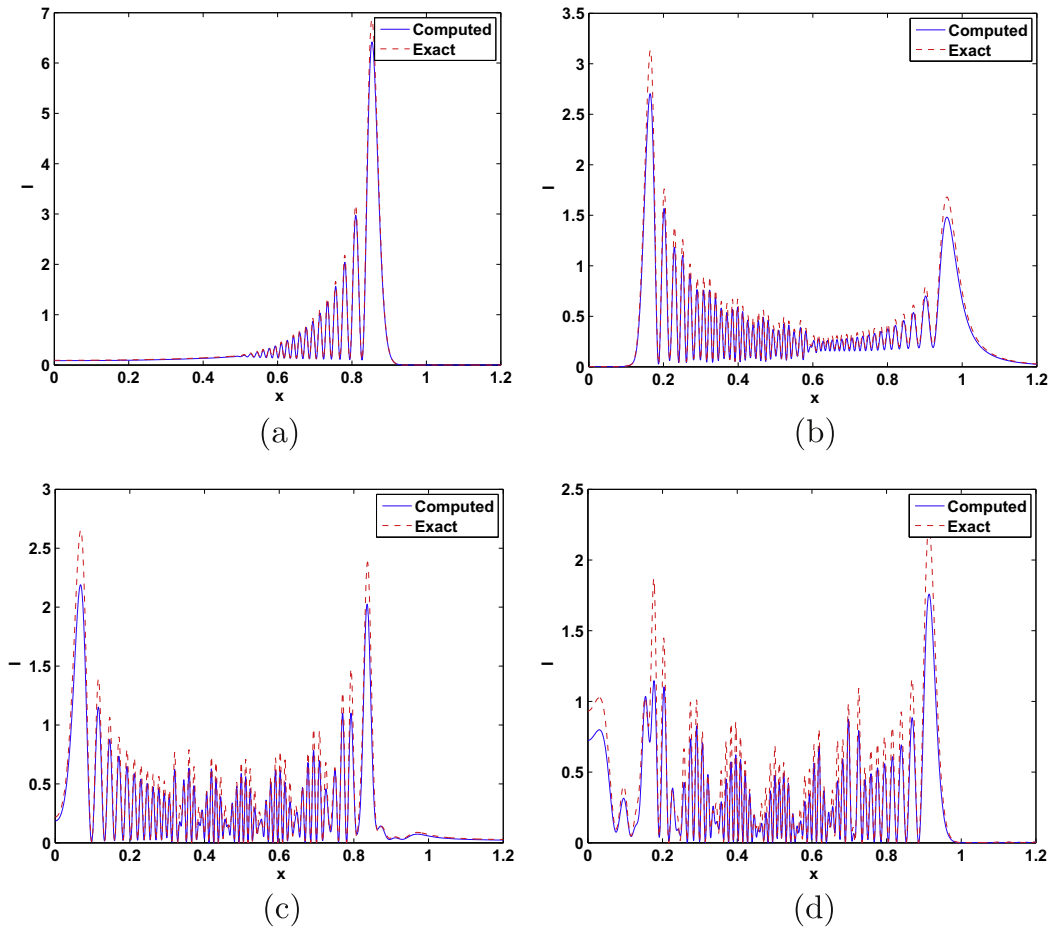

Fig. 12. (Example 5.2) Zoom-in of Fig. 11. $h = 1/64$ and the phase flow map step size $\Delta t = 0.40$. Eulerian Gaussian beam summations with beam reinitialization using the backward phase flow method on a mesh $I = J = 256$, $M = 2^{14} + 1$. The position densities at (a) $t = 5\Delta t = 2$, (b) $t = 10\Delta t = 4$, (c) $t = 15\Delta t = 6$, and (d) $t = 20\Delta t = 8$.

Concerning the computational complexity of the resulting algorithm in $\mathbf{R}^d$, we have the same order as in (52). Following the above argument, to accurately resolve the Gaussian $\exp[-\|x_{i'} - x_j\|^2/(2\hbar)]$ in the FBI transform, we require $\Delta x = O(\hbar^{1/2})$ and so $I = O(\hbar^{-d/2})$. The uncertainty principle (22) gives also $\Delta y = O(\hbar)$ and therefore $M = O(\hbar^{-d})$. To resolve the Gaussian of the FBI transform in the p-direction, we have also $\Delta p = O(\hbar^{1/2})$ and so $J = O(\hbar^{-d/2})$. All these estimates lead to $\alpha(I,J,M) = I \cdot (M/I) = \hbar^{-d}, \beta(I,J,M) = I \cdot (M/I) = \hbar^{-d}$, and therefore the overall computational complexity of the whole algorithm in the d-dimensions is $O(\hbar^{-d})$.

4. FBI-transform-based Gaussian beam global asymptotic solutions

Following the idea in [22,24], we prove that the beam solution defined in (18) is a global asymptotic solution to the initial value problem (1) and (2).

Theorem 4.1. *The solution (17) is a global asymptotic solution to the initial value problem (1) and (2) in the following sense: in a finite time interval [0,T], for* $\hbar$ *small enough,*

$$\|(-\imath\hbar\partial_t + H(x,-\imath\hbar\partial_x))U_\eta\|_{L^2(\mathbb{R}^d\times[0,T])} \leqslant C\sqrt{\mathrm{Vol}(G_\eta)}\|U_0\|_{L^2(\mathbb{R}^d)}\hbar^{\frac{3}{2}-\frac{d}{2}},$$
$$\lim_{\eta\to 0} U_\eta(x,0) = U_0(x),$$

where $H(x,p) = \frac{1}{2}p^2 + V(x)$ *is the Hamiltonian for the Schrödinger equation, and C is a constant independent of* $\hbar$.

To prove this theorem, we need some lemmas. In formulas (11) and (12) we define two global approximations to the phase and amplitude functions by using Taylor expansions centered on the x-projection of the bicharacteristic $\{(x(t;x_0,p_0),p(t;x_0,p_0)): t \geqslant 0\}$. We have the following estimates which are proved in [20].

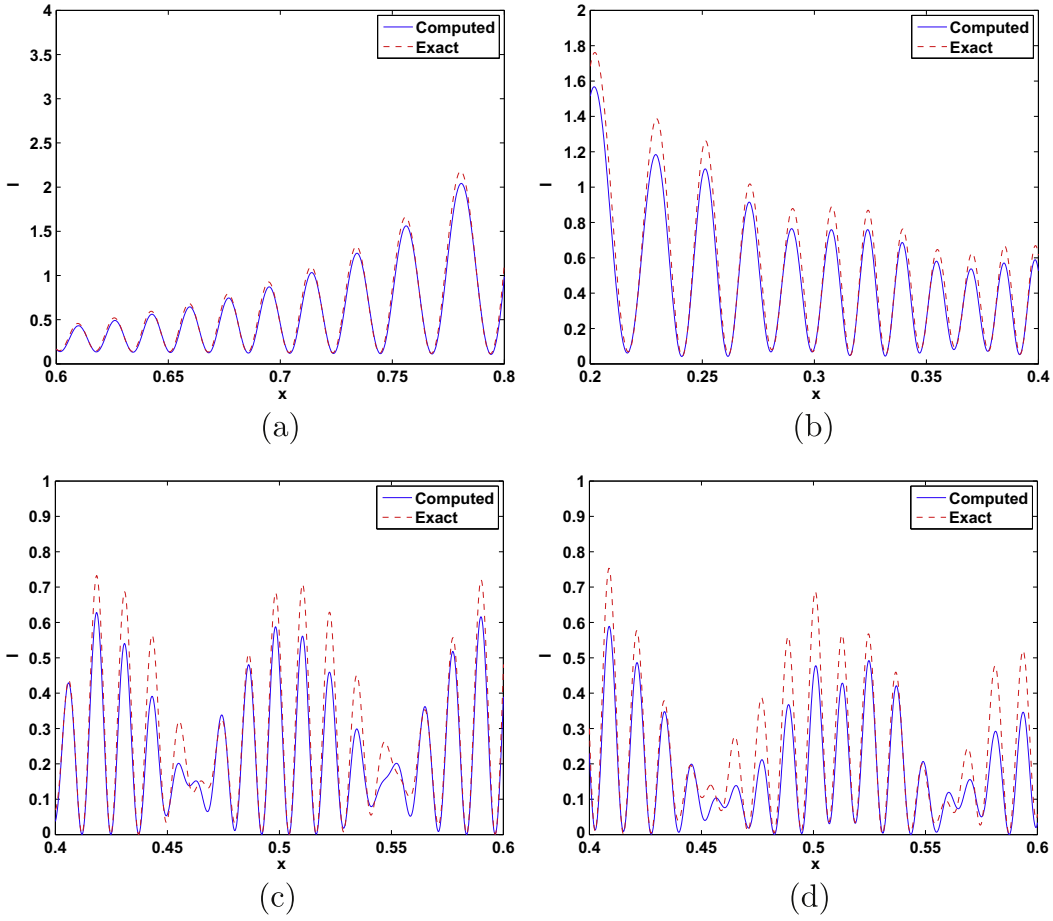

Fig. 13. (Example 5.2) Zoom-in of Fig. 12. $\hbar = 1/64$ and the phase flow map step size $\Delta t = 0.40$. Eulerian Gaussian beam summations with beam reinitialization using the backward phase flow method on a mesh $I = J = 256$, $M = 2^{14} + 1$. The position densities at (a) $t = 5\Delta t = 2$, (b) $t = 10\Delta t = 4$, (c) $t = 15\Delta t = 6$, and (d) $t = 20\Delta t = 8$.

Lemma 4.2. *Assume that the Hamiltonian is C^2 differentiable. Then the functions (11) and (12)* em satisfy the eikonal and transport equations in the following approximate sense, respectively:

$$\tau_t(x,t;x_0,p_0) + H(x,\tau_x(x,t;x_0,p_0)) = O(|x - x(t;x_0,p_0)|^3), \tag{54}$$

$$A_t(x,t;x_0,p_0) + H_p \cdot A_x + \frac{A}{2}\mathrm{trace}(\tau_{xx}) = O(|x - x(t;x_0,p_0)|), \tag{55}$$

where $H(x,p) = \frac{1}{2}p^2 + V(x)$.

We also need the following lemma which is proved in [22,24].

Lemma 4.3. *Assume that c (x,t) vanishes to order $S-1$ on $\gamma = \{(x(t),t): 0 \leqslant t \leqslant T\}$ which is the x-projection of a bicharacteristic $\{(x(t),p(t)) : 0 \leqslant t \leqslant T\}$, $supp(c) \cap \{(x,t) : x \in \mathbb{R}^d, 0 \leqslant t \leqslant T\}$ is compact, and Im $(\phi(x,t)) \geqslant a|x - x(t)|^2$ on $supp(c) \cap \{(x,t) : x \in \mathbb{R}^d, 0 \leqslant t \leqslant T\}$, where a is a positive constant. Then*

$$\int_0^T \int_{\mathbb{R}^d} \left| c(x,t) e^{\imath \frac{\phi(x,t)}{\hbar}} \right|^2 dx dt \leqslant C\hbar^{S+\frac{d}{2}}, \tag{56}$$

where C is a constant independent of $\hbar$.

Now we are ready to prove Theorem 4.1.

Proof. It is easy to show that at $t = 0$ we recover the initial data. Since

$$\Psi(x,0;x_0,p_0) = \widehat{U}(x_0,p_0;\hbar)\exp\left(\imath\frac{[\tau(x,0;x_0,p_0) - x_0 \cdot p_0]}{\hbar}\right)$$

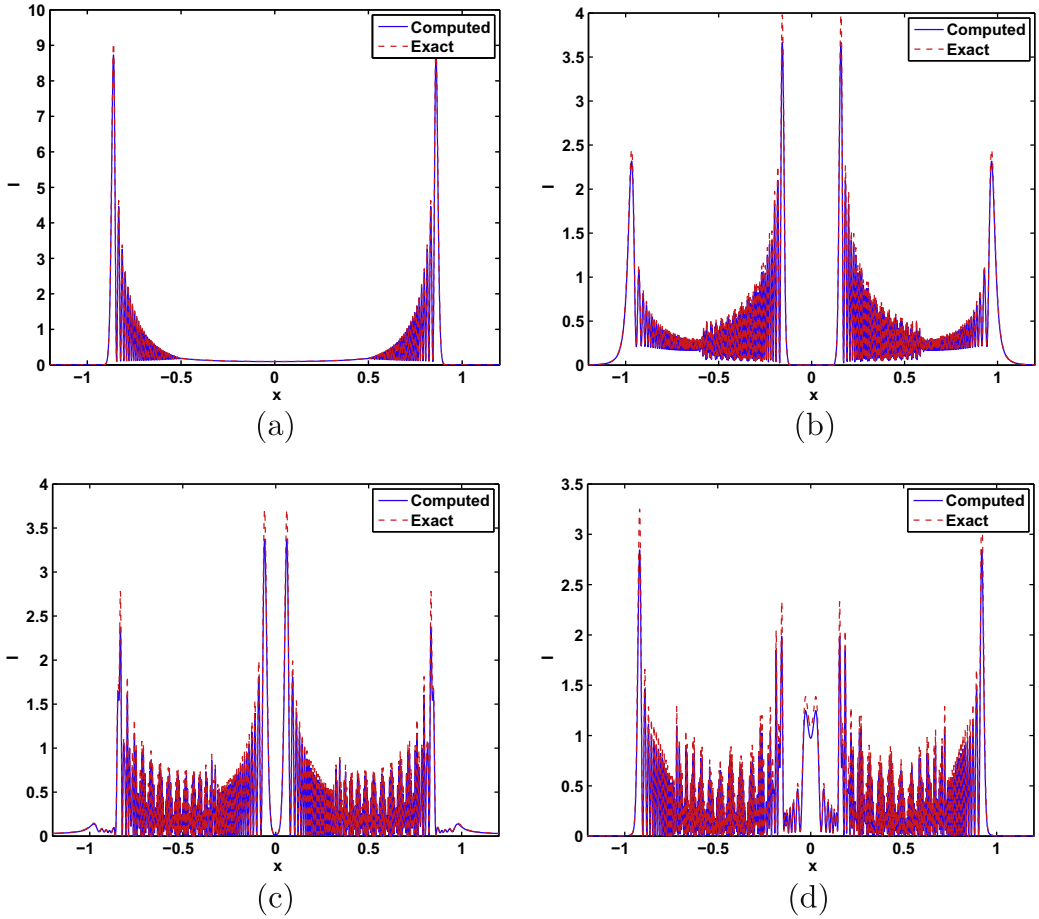

Fig. 14. (Example 5.2) $h = 1/128$ and the phase flow map step size $\Delta t = 0.40$. Eulerian Gaussian beam summations with beam reinitialization using the backward phase flow method on a mesh $I = J = 256$, $M = 2^{14} + 1$. The position densities at (a) $t = 5\Delta\ t = 2$, (b) $t = 10\Delta t = 4$, (c) $t = 15\Delta t = 6$, and (d) $t = 20\ \Delta t = 8$.

where

$$\tau(x,0;x_0,p_0) = p_0\cdot x_0 + p_0\cdot(x-x_0) + \frac{\imath}{2}(x-x_0)^T(x-x_0),$$

we have as $\eta \to 0$,

$$\begin{aligned} U_\eta(x,0) &= \alpha_{d,h}\int_{(x_0,p_0)\in\Omega_\eta} \Psi(x,0;x_0,p_0)dx_0dp_0 \\ &= \alpha_{d,h}\int_{\Omega_\eta} \hat{U}_0(x_0,p_0;\hbar)\exp\left[-\frac{\imath}{\hbar}(x_0-x)\cdot p_0 - \frac{(x_0-x)^2}{2\hbar}\right]dx_0dp_0 \\ &\to \alpha_{d,h}\int_{x_0}\int_{p_0} \hat{U}_0(x_0,p_0;\hbar)\exp\left[-\frac{\imath}{\hbar}(x_0-x)\cdot p_0 - \frac{(x_0-x)^2}{2\hbar}\right]dx_0dp_0 = \mathcal{T}^*\mathcal{T}U_0 = U_0, \end{aligned}$$

where $\mathcal{T}^*$ is the adjoint of $\mathcal{T}$. Here we have used a property of the FBI transform [15]: $\mathcal{T}^*\mathcal{T} = I$ under some appropriate conditions, where I is the identity operator.

Next we evaluate the following,

$$\begin{aligned} (-\imath\hbar\partial_t + H(x,-\imath\hbar\partial_x))U_\eta &= \alpha_{d,h}\int_{\Omega_\eta}(-\imath\hbar\partial_t + H(x,-\imath\hbar\partial_x))\Psi(x,t;x_0,p_0)dx_0dp_0 \\ &= \alpha_{d,h}\int_{\Omega_\eta}(\tau_t + H(x,\tau_x))A\exp\left(\imath\frac{\tau(x,t;x_0,p_0)}{\hbar}\right)dx_0dp_0 \\ &\quad + \alpha_{d,h}\int_{\Omega_\eta}\frac{\hbar}{\imath}\left(A_t + H_p\cdot A_x + \frac{A}{2}\mathrm{trace}(\tau_{xx})\right)\exp\left(\imath\frac{\tau(x,t)}{\hbar}\right)dx_0dp_0 \equiv f_1(x,t) + f_2(x,t). \end{aligned}$$

We estimate f_1 first. By the Cauchy–Schwartz inequality, we have

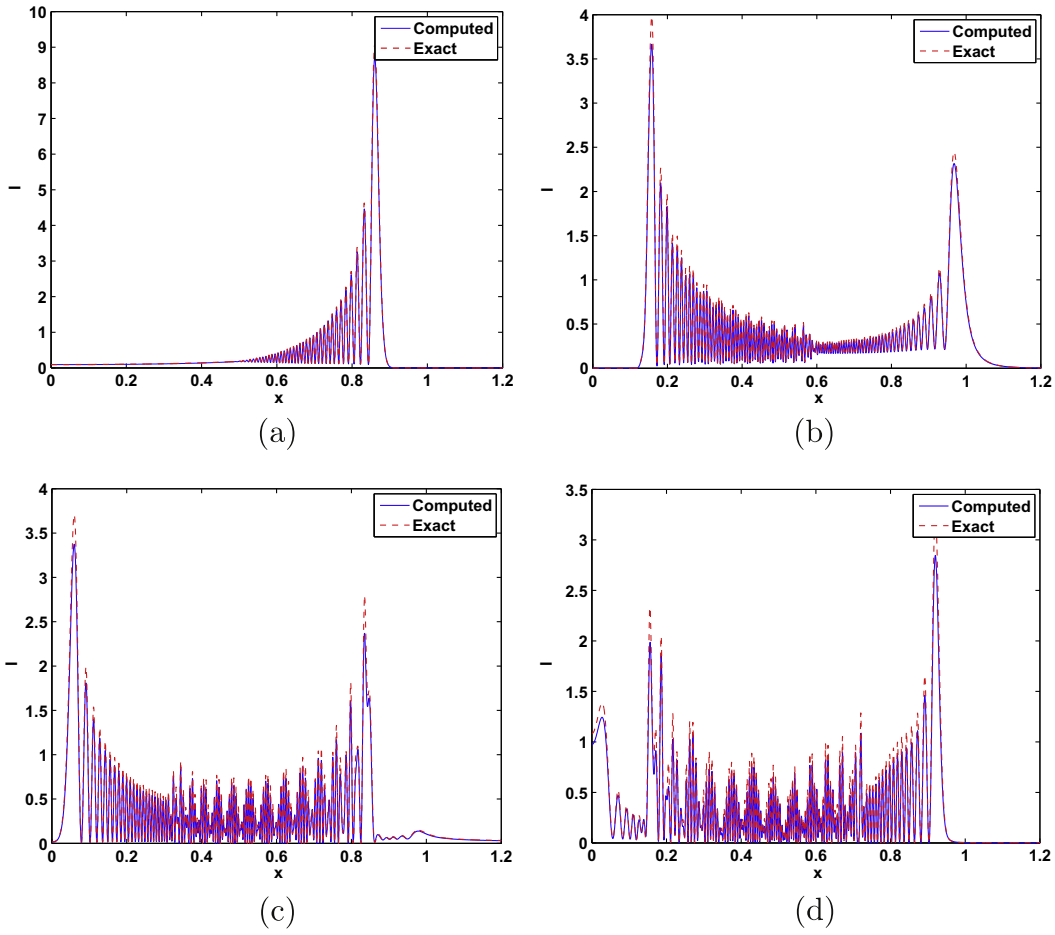

Fig. 15. (Example 5.2) Zoom-in of Fig. 14. $h = 1/128$ and the phase flow map step size $\Delta t = 0.40$. Eulerian Gaussian beam summations with beam reinitialization using the backward phase flow method on a mesh $I = J = 256$, $M = 2^{14}+1$. The position densities at (a) $t = 5\Delta t = 2$, (b) $t = 10\Delta t = 4$, (c) $t = 15\Delta t = 6$, and (d) $t = 20\Delta t = 8$.

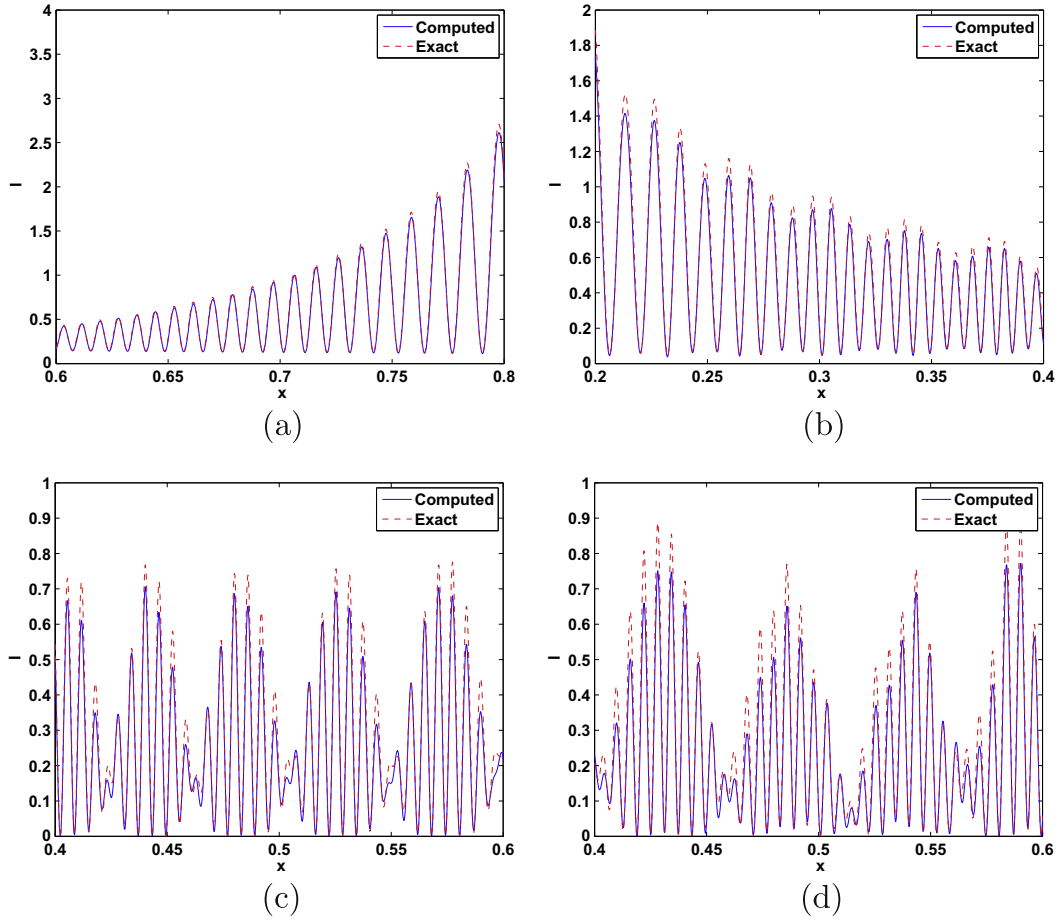

Fig. 16. (Example 5.2) Zoom-in of Fig. 15. $h = 1/128$ and the phase flow map step size $\Delta t = 0.40$. Eulerian Gaussian beam summations with beam reinitialization using the backward phase flow method on a mesh $I = J = 256$, $M = 2^{14} + 1$. The position densities at (a) $t = 5\Delta t = 2$, (b) $t = 10\Delta t = 4$, (c) $t = 15\Delta t = 6$, and (d) $t = 20\Delta t = 8$.

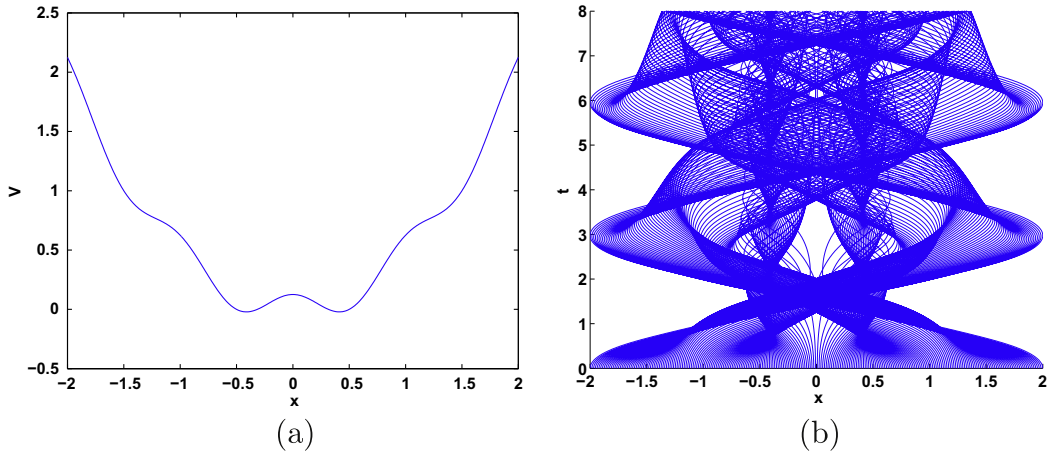

Fig. 17. (Example 5.3) (a) The Cosine-Quadratic potential and (b) the complicated ray structure up to time $t = 8$.

$$|f_1(x,t)|^2 = \left| \alpha_{d,h} \int_{\Omega_\eta} \frac{(\tau_t + H(x,\tau_x))\widehat{U}_0(x_0,p_0;\hbar)}{\sqrt{\det C(t;x_0,p_0)}} \exp\left(\imath \frac{[\tau(x,t;x_0,p_0) - x_0 \cdot p_0]}{\hbar}\right) dx_0 dp_0 \right|^2$$
$$\leqslant \alpha_{d,h}^2 \|U_0\|_{L^2(\mathbb{R}^d)}^2 \int_{\Omega_\eta} \left| \frac{(\tau_t + H(x,\tau_x))}{\sqrt{\det C(t;x_0,p_0)}} \exp\left(\imath \frac{[\tau(x,t;x_0,p_0) - x_0 \cdot p_0]}{\hbar}\right) \right|^2 dx_0 dp_0,$$

where we have used another property of the FBI transform: $\|\widehat{U}_0\|^2_{L^2(\mathbb{R}^{2d})} = \|U_0\|^2_{L^2(\mathbb{R}^d)}$.

Denoting $L^2(\mathbb{R}^d \times [0,T]) = L^2_{x,t}$ we have

$$\|f_1\|^2_{L^2_{x,t}} \leqslant \alpha^2_{d,h}\|U_0\|^2_{L^2(\mathbb{R}^d)} \times \int_{\Omega_\eta}\int_0^T \int_{\mathbb{R}^d_x} \left| \frac{(\tau_t + H(x,\tau_x))}{\sqrt{\det C(t;x_0,p_0)}} \exp\left(\imath \frac{[\tau(x,t;x_0,p_0) - x_0 \cdot p_0]}{\hbar}\right)\right|^2 dx dt dx_0 dp_0$$
$$\leqslant C^2 \alpha^2_{d,h}\|U_0\|^2_{L^2(\mathbb{R}^d)} \mathrm{Vol}(\Omega_\eta)\hbar^{3+\frac{d}{2}},$$

where we have used Lemma 4.2 and 4.3 with $S = 3$ in the last step. Thus taking into account the definition of $\alpha_{d,h}$ we have

$$\|f_1\|_{L^2(\mathbb{R}^d\times[0,T])} \leqslant C\sqrt{\mathrm{Vol}(\Omega_\eta)}\|U_0\|_{L^2(\mathbb{R}^d)}\hbar^{\frac{3}{2}-\frac{d}{2}}.$$

Similarly, using Lemma 4.2 and 4.3 with $S = 1$ we have the estimate for f_2,

$$\|f_2\|_{L^2(\mathbb{R}^d\times[0,T])} \leqslant C\sqrt{\mathrm{Vol}(\Omega_\eta)}\|U_0\|_{L^2(\mathbb{R}^d)}\hbar^{\frac{3}{2}-\frac{d}{2}},$$

where C is a constant independent of $\hbar$. Combining the estimates for f_1 and f_2, we have the results stated in the theorem. □

We remark in passing that this in turn proves that the beam solution defined in (29) is also an asymptotic solution because the solution (29) is obtained from the solution (17) by using the phase flow map; see [11] for more details.

We also remark that by using optimal norms of some approximation operators defined by the beam summation operator as introduced in [3], one may easily improve the asymptotic rate to be $\hbar^{\frac{3}{2}}$. We will report on this in an upcoming paper.

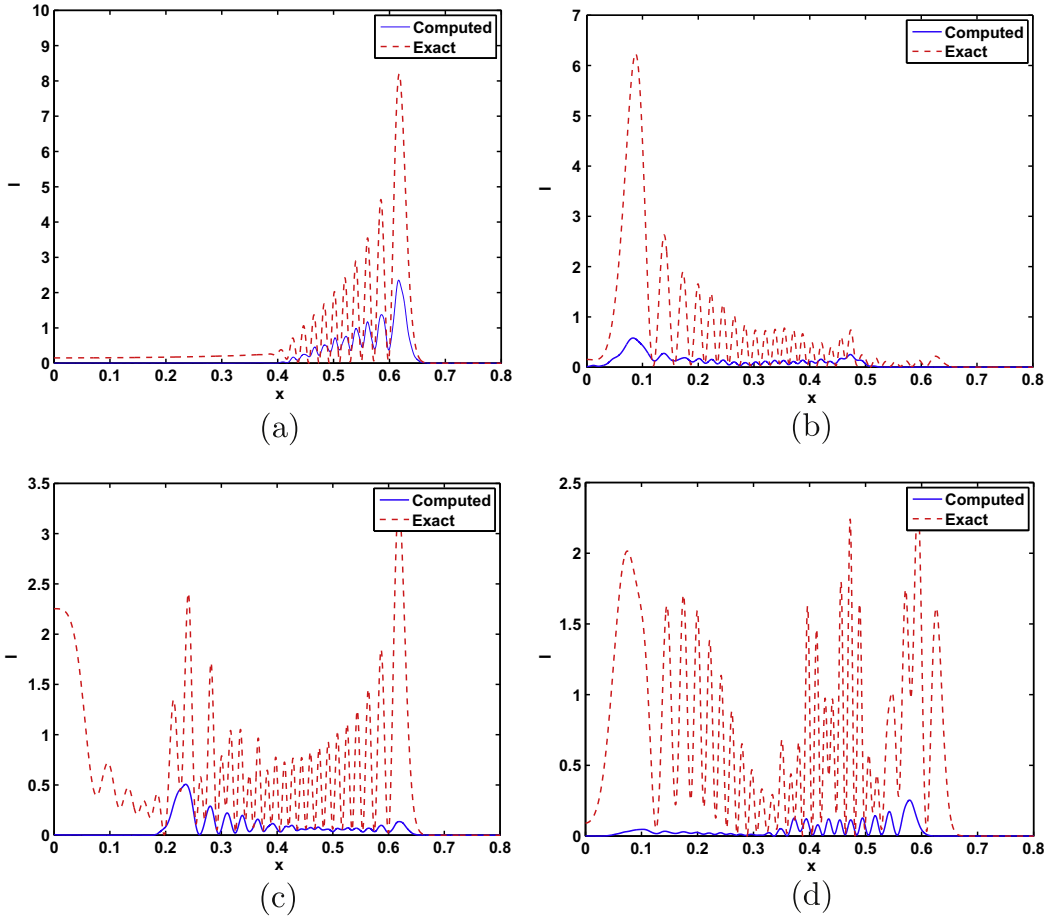

Fig. 18. (Example 5.3) $\hbar = 1/64$ and the phase flow map step size $\Delta t = 2.0$. Eulerian Gaussian beam summations with beam reinitialization using the backward phase flow method on a mesh $I = J = 256$, $M = 2^{14} + 1$. The position densities at (a) $t = \Delta\, t = 2$, (b) $t = 2\Delta t = 4$, (c) $t = 3\Delta t = 6$, and (d) $t = 4\Delta\, t = 8$.

5. Numerical examples

We show some numerical examples to validate our algorithms. Since the wave function is an auxiliary quantity used to compute physical observables, such as the position density,

$$I(x,t) = |U(x,t)|^2, \tag{57}$$

we will use this quantity to justify our algorithms.

According to the proposed algorithm, we first obtain all the required mappings on a fixed uniform mesh. The resulting mappings allow us to construct accurate semi-classical solutions for $\hbar$'s in a certain interval as shown in the following examples.

Since an exact wave function for the Schrödinger equation is not available in general, we will first use a pseudo-spectral method [19,2] to solve the equation directly to obtain an "*exact*" wave function and then use the resulting position density to calibrate our beam solutions. Because such pseudo-spectral methods are independent of the semi-classical asymptotics and can yield highly accurate solutions for a long period of time, it is reasonable to use such solutions to calibrate our Gaussian-beam-based semi-classical solutions up to a large time.

5.1. Example 1: Morse potential

We consider the Morse potential given by [5,7]

$$V = D[1 - \exp(-\lambda x)]^2, \tag{58}$$

where $D = 160$ and $\lambda = 0.036$; see Fig. 2(a). The initial particle is a Gaussian centered at $x = 2$ with standard deviation of $\sigma_0 = \frac{1}{2\sqrt{6}}$ with zero initial momentum $p_0 = 0$ [5,7]:

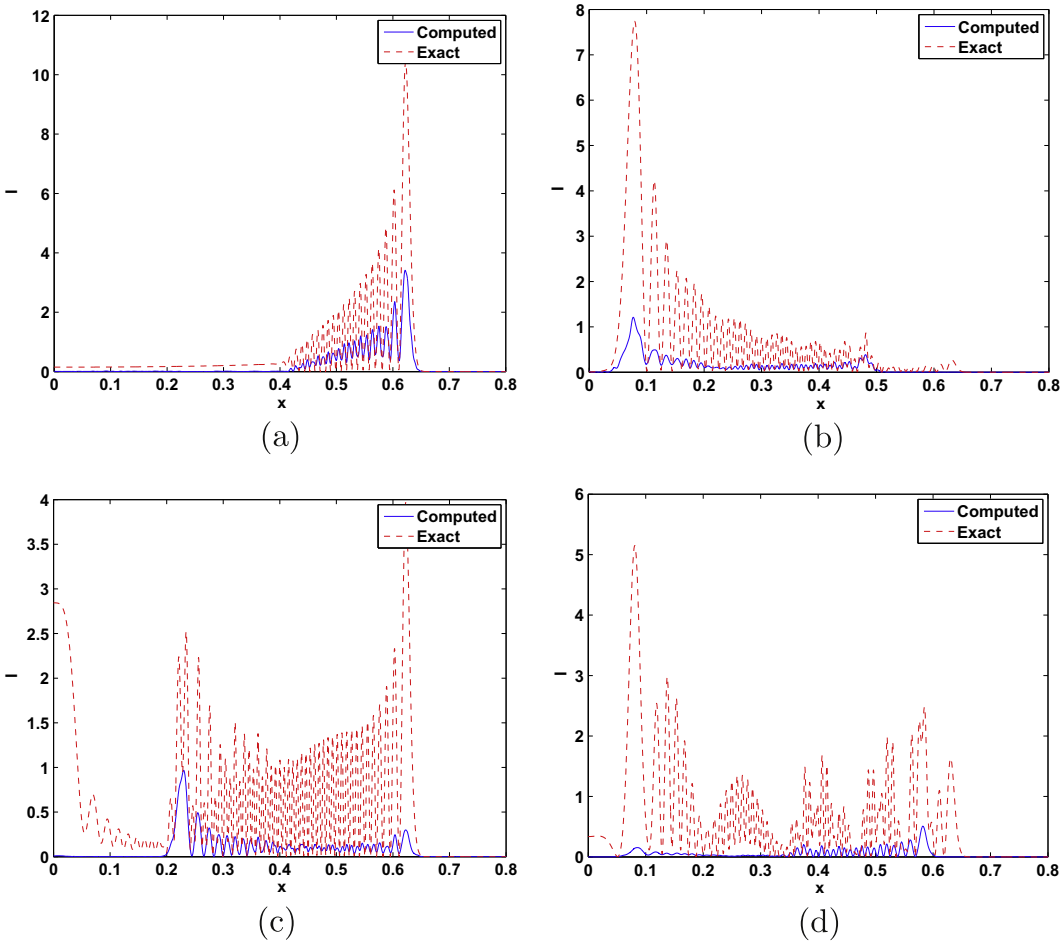

Fig. 19. (Example 5.3) $\hbar = 1/128$ and the phase flow map step size $\Delta t = 2.0$. Eulerian Gaussian beam summations with beam reinitialization using the backward phase flow method on a mesh $I = J = 256$, $M = 2^{14} + 1$. The position densities at (a) $t = \Delta\ t = 2$, (b) $t = 2\Delta t = 4$, (c) $t = 3\Delta t = 6$, and (d) $t = 4\Delta\ t = 8$.

$$U|_{t=0} = \frac{1}{\sqrt{\sigma_0\sqrt{2\pi}}} \exp\left(-\frac{(x-2)^2}{4\sigma_0^2}\right) \exp\left(-\frac{ix\cdot p_0}{\hbar}\right). \tag{59}$$

To illustrate the potential difficulty of this example, in Fig. 2(b) we plot some rays traced according to a subset of the initial values used in the FBI-based Eulerian beam construction which is formulated in phase space. We compute the solution up to $T = 15$.

We first take $\hbar = \frac{1}{32}$ to compute the semiclassical solution with different backward phase flow maps. Here the log time $\hat{t} = \log(1/\hbar) = 3.4657$. Fig. 3 shows the solutions at $t = 3, 6, \ldots, 15$ using a backward phase flow map with $\Delta t = 1.5$ on a mesh of $I = J = 256$ and $M = 2^{11} + 1$. This implies that Fig. 3(e) is obtained by applying beam reinitialization nine times. We compare our solutions with the *exact* solutions on a very fine mesh. These two solutions match very well even for long-time propagation. We next repeat the same example using a backward phase flow map with $\Delta t = 3.0$ and we plot the solutions at $t = 3, 6, \ldots, 15$ in Fig. 4. Fig. 4(a) shows that the computed solution at $t = 3$ matches with the *exact* solution very well and we do not see visual differences in comparison to Fig. 3(a). However, as time increases, the errors in the solution propagate and build up. The solution at the final time $T = 15$ is noticeably different from the *exact* solution.

We also take $\hbar = \frac{1}{128}$ to compute the semiclassical solution with different backward phase flow maps. Here the log time $\hat{t} = \log(1/\hbar) = 4.8520$. Fig. 5 shows the solutions at $t = 3, 6, \ldots, 15$ using a backward phase flow map with $\Delta t = 1.5$ on a mesh of $I = J = 1025$ and $M = 2^{11} + 1$. This implies that Fig. 5(e) is obtained by applying beam reinitialization nine times. We compare our solutions with the *exact* solutions on a very fine mesh. These two solutions match very well even for long-time propagation. We also repeat the same example using a backward phase flow map with $\Delta t = 3.0$ and we plot the solutions at $t = 3, 6, \ldots, 15$ in Fig. 6. Because of the smaller $\hbar$, we do not see noticeable differences between the two beam solutions based on different backward phase flow maps.

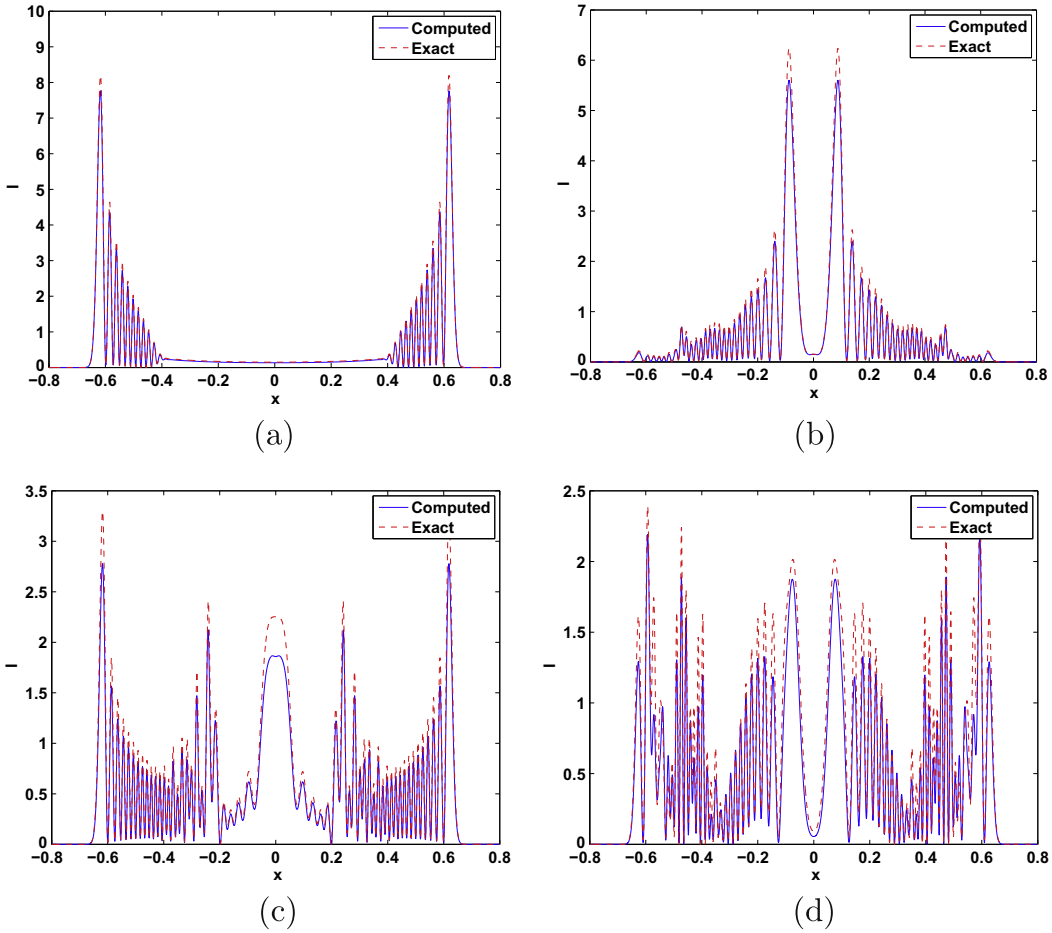

Fig. 20. (Example 5.3) $\hbar = 1/64$ and the phase flow map step size $\Delta t = 0.40$. Eulerian Gaussian beam summations with beam reinitialization using the backward phase flow method on a mesh $I = J = 256$, $M = 2^{14} + 1$. The position densities at (a) $t = 5\Delta$ $t = 2$, (b) $t = 10\Delta t = 4$, (c) $t = 15\Delta t = 6$, and (d) $t = 20$ $\Delta t = 8$.

5.2. Example 2: a gaussian in a cosine potential field

The potential is given by

$$V(x) = \frac{1}{8}\cos(2\pi x). \tag{60}$$

The initial profile is a Gaussian of standard deviation $\sigma_0 = 0.1$ centered at $x = 0$ with zero initial momentum $p_0 = 0$:

$$U|_{t=0} = \frac{1}{\sqrt{\sigma_0\sqrt{2\pi}}}\exp\left(-\frac{x^2}{4\sigma_0^2}\right)\exp\left(-\frac{\imath x\cdot p_0}{h}\right). \tag{61}$$

Since the potential is a hill at $x = 0$, we expect that the Gaussian will split into two and each of them will fall into one of the potential wells centered at $x = \pm 0.5$, respectively. To illustrate the potential difficulty of this example, in Fig. 7 we plot some rays traced according to a subset of the initial values used in the FBI-based Eulerian beam construction. We compute the Eulerian Gaussian beam solution up to the final time $T = 8$.

Since the Hessian of the potential is bounded by

$$V_{xx} = -\frac{\pi^2}{2}\cos(2\pi x) \geqslant -\frac{\pi^2}{2}, \tag{62}$$

the beam width could grow in the order of $O[\exp(\pi t/\sqrt{2})]$. In order to keep the beam width to be of order $O(\sqrt{h})$, according to Eq. (33) we require

$$\exp\left(\sqrt{\frac{\pi^2}{2}}\Delta t\right) = \sqrt{2}\pi, \tag{63}$$

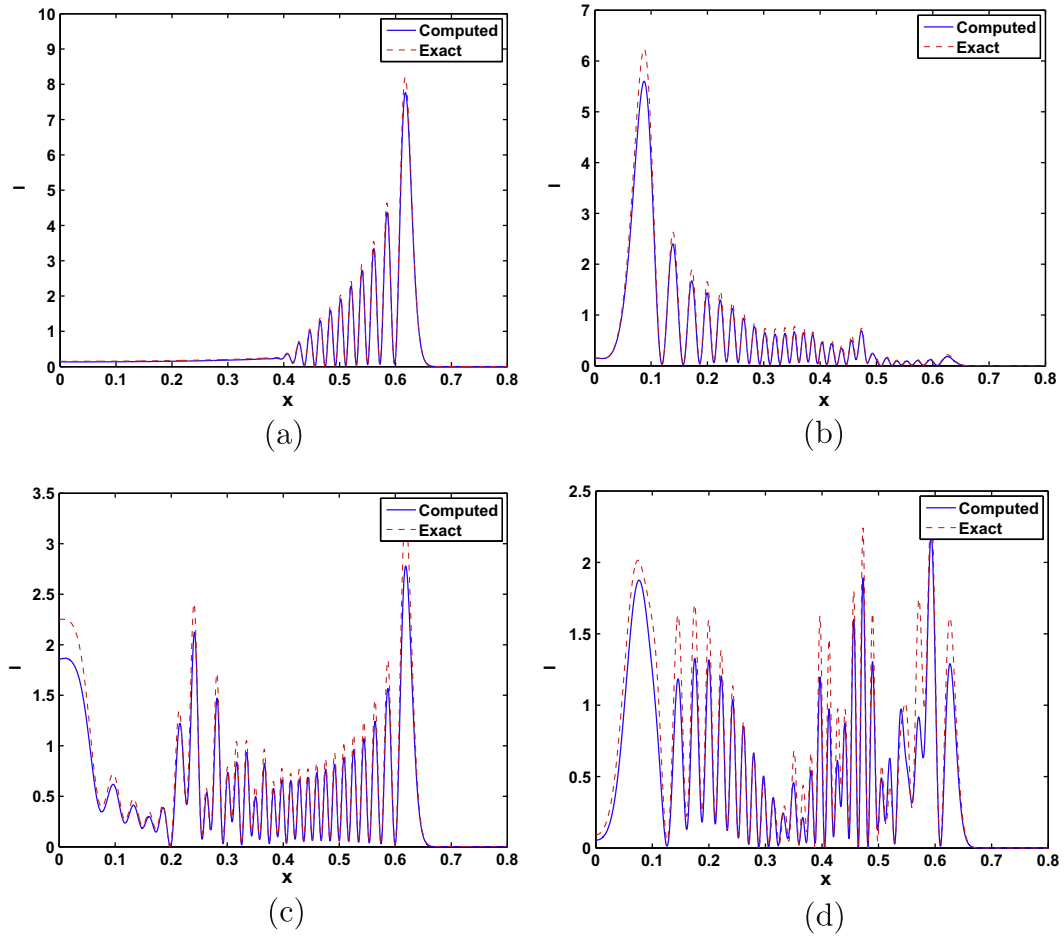

Fig. 21. (Example 5.3) Zoom-in of Fig. 20. $h = 1/64$ and the phase flow map step size $\Delta t = 0.40$. Eulerian Gaussian beam summations with beam reinitialization using the backward phase flow method on a mesh $I = J = 256$, $M = 2^{14} + 1$. The position densities at (a) $t = 5\Delta\ t = 2$, (b) $t = 10\Delta t = 4$, (c) $t = 15\Delta t = 6$, and (d) $t = 20\ \Delta t = 8$.

which implies that the size Δt for constructing the backward phase flow map should be at most

$$\Delta t^* = \frac{\sqrt{2}}{\pi} \ln\left(\sqrt{2}\pi\right) \simeq 0.6713. \tag{64}$$

Fig. 8 shows the solution at the final time $T = 8$ on a mesh of $I = J = 256$ and $M = 2^{14} + 1$ *without* any beam reinitialization for $\hbar = 1/64$ and $\hbar = 1/128$, respectively. In the case of $\hbar = 1/64$, the log time $\hat{t} = 4.1589$; in the case of $\hbar = 1/128$, the log time $\hat{t} = 4.8520$. We compare these beam solutions with the *exact* solutions. The beam solutions are significantly different from the exact solution. Even if we halve the value of $\hbar$, the computed solution does not improve too much.

To demonstrate improvement in the solutions by applying beam reinitialization, we apply the backward phase flow method of step size $\Delta t = 2.0$ on a mesh of $I = J = 256$ and $M = 2^{14} + 1$, and we reinitialize the beam computation at the beginning of each interval of $\Delta t = 2$. Note that this step size is larger than the estimated step size; i.e. $\Delta t > \Delta t^*$. We show the solutions with $\hbar = 1/64$ and $\hbar = 1/128$ at different times in Figs. 9 and 10, respectively. Fig. 9(d) and Fig. 10(d) show the solutions at $t = 8$ and they are improved slightly in comparison to the corresponding solutions as in Fig. 8. However, since $\Delta t > \Delta t^*$, we do not expect that beam summation will give accurate approximations.

Next we choose the size of the backward phase flow map to be $\Delta t < \Delta t^*$. In Figs. 11–13, we construct the solutions for $\hbar = 1/64$ at $t = 2, 4, 6$ and 8 based on the backward phase flow map on a mesh of $I = J = 256$ and $M = 2^{14} + 1$ with $\Delta t = 0.4$ which is smaller than Δt^*. This implies that the solution at $t = 2$ is obtained by applying beam reinitialization four times at $t = 0.4, 0.8$, 1.2 and 1.6. We also compare our computed solutions with the *exact* solutions obtained by using a direct numerical method on a very fine mesh. In Figs. 12 and 13, we plot only the solutions in the positive x region to see the differences between beam and exact solutions more clearly.

To further demonstrate the property of the algorithm, we decrease $\hbar$. In Figs. 14–16, we construct the solutions for $\hbar = 1/128$ at $t = 2, 4, 6$ and 8 based on the backward phase flow map on a mesh of $I = J = 256$ and $M = 2^{14} + 1$ with $\Delta t = 0.4$. This implies that the solution at $t = 2$ is obtained by applying beam reinitialization four times at $t = 0.4, 0.8, 1.2$ and 1.6. We also

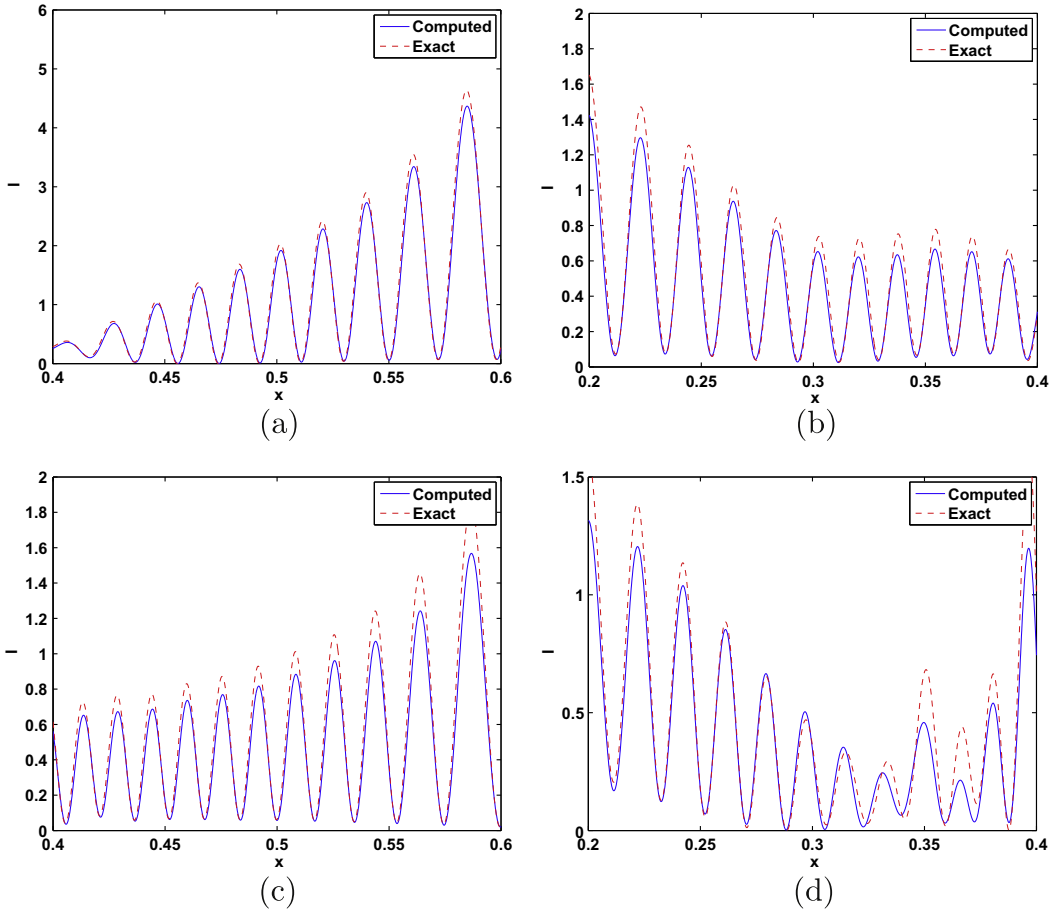

Fig. 22. (Example 5.3) Zoom-in of Fig. 21. $\hbar = 1/64$ and the phase flow map step size $\Delta t = 0.40$. Eulerian Gaussian beam summations with beam reinitialization using the backward phase flow method on a mesh $I = J = 256, M = 2^{14} + 1$. The position densities at (a) $t = 5\Delta$ $t = 2$, (b) $t = 10\Delta t = 4$, (c) $t = 15\Delta t = 6$, and (d) $t = 20$ $\Delta t = 8$.

compare our computed solutions with the *exact* solutions obtained by using a direct numerical method on a very fine mesh. In Figs. 15 and 16, we plot only the solutions in the positive x region to see the differences between beam and exact solutions more clearly. As shown in Figs. 14–16, our beam solutions match very nicely with the *exact* solutions. This is reasonable since the Gaussian beam approximation is an asymptotic method to solve the Schrödinger equation in the semi-classical regime as $\hbar$ going to zero.

5.3. Example 3: a Gaussian in a Cosine-Quadratic potential field

The potential is given by

$$V(x) = \frac{1}{8}\cos(2\pi x) + \frac{1}{2}x^2. \tag{65}$$

The initial profile is a Gaussian of standard deviation $\sigma_0 = 0.1$ centered at $x = 0$ with zero initial momentum $p_0 = 0$:

$$U|_{t=0} = \frac{1}{\sqrt{\sigma_0\sqrt{2\pi}}}\exp\left(-\frac{x^2}{4\sigma_0^2}\right)\exp\left(-\frac{\imath x\cdot p_0}{\hbar}\right). \tag{66}$$

Since the potential is a hill at $x = 0$, we expect that the Gaussian will split into two and each of them will fall into one of the potential wells centered at $x = \pm 0.5$, respectively; see Fig. 17(a). To illustrate the potential difficulty of this example, in Fig. 17(b) we plot some rays traced according to a subset of initial values used in the FBI-based Eulerian beam construction. We compute the Eulerian Gaussian beam solution up to the final time $T = 8$.

Since the Hessian of the potential is bounded by

$$V_{xx} = -\frac{\pi^2}{2}\cos(2\pi x) + 1 \geqslant -\frac{\pi^2}{2} + 1, \tag{67}$$

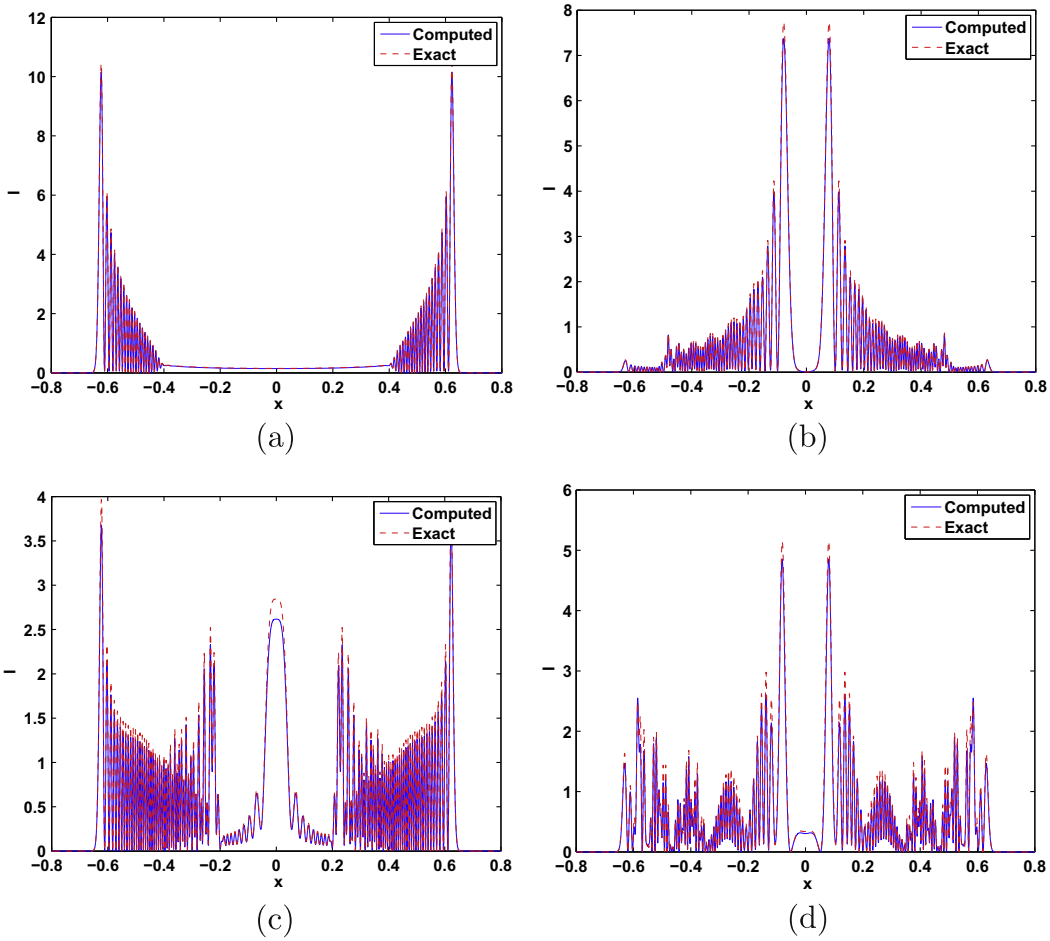

Fig. 23. (Example 5.3) $h = 1/128$ and the phase flow map step size $\Delta t = 0.40$. Eulerian Gaussian beam summations with beam reinitialization using the backward phase flow method on a mesh $I = J = 256$, $M = 2^{14} + 1$. The position densities at (a) $t = 5\Delta\, t = 2$, (b) $t = 10\Delta t = 4$, (c) $t = 15\Delta t = 6$, and (d) $t = 20\ \Delta t = 8$.

the beam width could grow in the order of $O\left[\exp\left(\sqrt{\pi^2/2+1}t\right)\right]$. In order to keep the beam width of order $O(\sqrt{\hbar})$, we require that

$$\exp\left(\Delta t\sqrt{\frac{\pi^2}{2}+1}\right)=\sqrt{2}\pi \tag{68}$$

which implies that the step size Δt for constructing the backward phase flow map be at most

$$\Delta t^*=\ln\left(\sqrt{2}\pi\right)/\sqrt{\frac{\pi^2}{2}+1}\simeq 0.7518. \tag{69}$$

To demonstrate improvement in the solutions by applying beam reinitialization, we apply the backward phase flow method of step size $\Delta t = 2.0$ on a mesh of $I = J = 256$ and $M = 2^{14} + 1$, and we reinitialize beam computation at the beginning of each interval of $\Delta t = 2$. Note that this step size is larger than the estimated step size; i.e. $\Delta t > \Delta t^*$. We show the solutions with $\hbar = 1/64$ and $\hbar = 1/128$ at different times in Figs. 18 and 19, respectively. However, since $\Delta t > \Delta t^*$, we do not expect that beam summation will give accurate approximations.

In Figs. 20–22, we construct the solutions for $\hbar = 1/64$ at $t = 2, 4, 6$ and 8 based on the backward phase flow map on a mesh of $I = J = 256$ and $M = 2^{14} + 1$ with $\Delta t = 0.4$ which is smaller than Δt^*. This implies that the solution at $t = 2$ is obtained by applying beam reinitialization four times at $t = 0.4, 0.8, 1.2$ and 1.6. We also compare our computed solutions with the "exact" solutions obtained by using a direct method on a very fine mesh. In Figs. 21 and 22, we plot only the solutions in the positive x region to see the differences between beam and exact solutions more clearly.

For a smaller $\hbar = 1/128$, as shown in Figs. 23–25, our beam solutions match very nicely with the *exact* solutions.

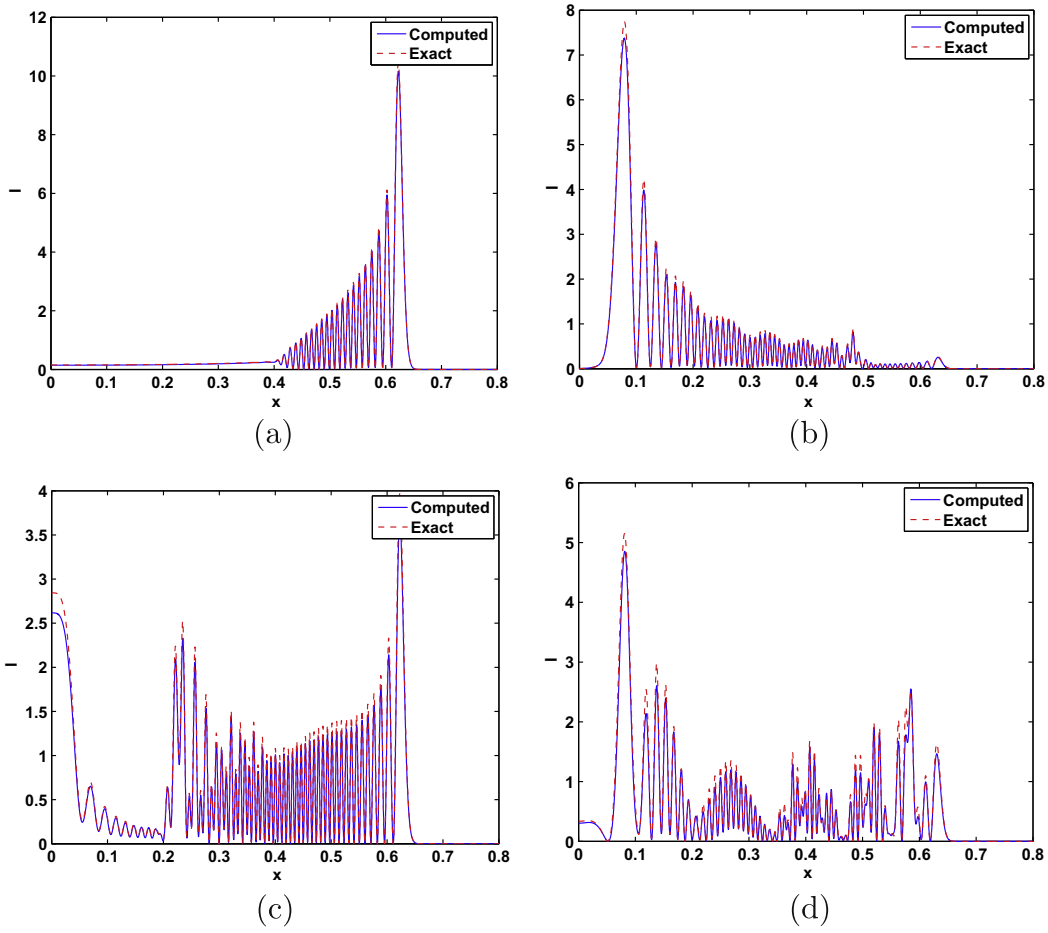

Fig. 24. (Example 5.3) Zoom-in of Fig. 23. $\hbar = 1/128$ and the phase flow map step size $\Delta t = 0.40$. Eulerian Gaussian beam summations with beam reinitialization using the backward phase flow method on a mesh $I = J = 256$, $M = 2^{14} + 1$. The position densities at (a) $t = 5\Delta$ $t = 2$, (b) $t = 10\Delta t = 4$, (c) $t = 15\Delta t = 6$, and (d) $t = 20$ $\Delta t = 8$.

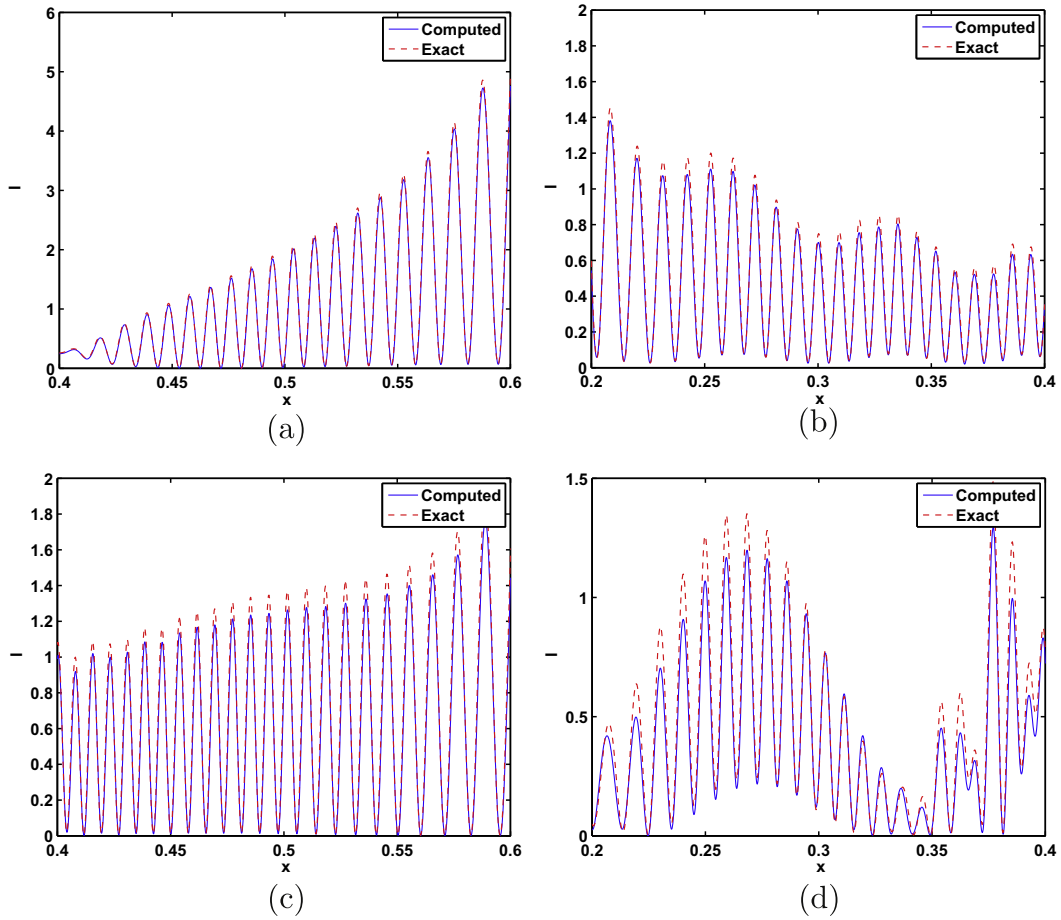

Fig. 25. (Example 5.3) Zoom-in of Fig. 24. $h = 1/128$ and the phase flow map step size $\Delta t = 0.40$. Eulerian Gaussian beam summations with beam reinitialization using the backward phase flow method on a mesh $I = J = 256$, $M = 2^{14} + 1$. The position densities at (a) $t = 5\Delta\ t = 2$, (b) $t = 10\Delta t = 4$, (c) $t = 15\Delta t = 6$, and (d) $t = 20\ \Delta t = 8$.

6. Conclusions

We proposed the backward phase flow method to implement the FBI-transform-based Eulerian Gaussian beams to solve the Schrödinger equation in the semi-classical regime. In this paper we aimed at two challenging computational issues of the Eulerian Gaussian beam method: how to carry out long-time beam propagation and how to compute beam ingredients rapidly in phase space. By virtue of the FBI transform, we addressed the first issue by introducing the reinitialization strategy into the Eulerian Gaussian beam framework. Essentially we reinitialize the beam propagation by applying the FBI transform to wavefields at intermediate time steps when the beams become too wide. To address the second issue, inspired by the original phase flow method, we proposed the backward phase method which allows us to compute beam ingredients rapidly. Numerical examples demonstrated the efficiency and accuracy of the proposed algorithms.

Acknowledgements

Leung was supported in part by the RGC under Grant DAG09/10.SC02. Qian would like to thank Professors R. Burridge, S. Osher and J. Ralston for their interests and encouragement in this work. Qian is in part supported by NSF DMS-0810104 and NSF DMS-0830161, and in part by AFOSR Grant #FA9550-04-1-0143.

References

[1] V.M. Babich, V.S. Buldyrev, Asymptotic Methods in Short Wave Diffraction Problems, Nauka, Moscow, 1972 (in Russian).
[2] W. Bao, S. Jin, P. Markowich, On time-splitting spectral approximations for the Schrödinger equation in the semiclassical regime, J. Comput. Phys. 175 (2002) 487–524.
[3] S. Bougacha, J. Akian, R. Alexandre, Gaussian beams summation for the wave equation in a convex domain, Commun. Math. Sci. 7 (2009) 973–1008.

[4] V. Cerveny, M. Popov, I. Psencik, Computation of wave fields in inhomogeneous media-Gaussian beam approach, Geophys. J.R. Astr. Soc. 70 (1982) 109–128.
[5] E. Heller, Cellular dynamics: a new semiclassical approach to time-dependent quantum mechanics, J. Chem. Phys. 94 (1991) 2723–2729.
[6] E. Heller, Guided Gaussian wave packets, Acc. Chem. Res. 39 (2006) 127–134.
[7] E. Heller, S. Tomsovic, M. Sepulveda, Time domain approach to semiclassical dynamics: breaking the log time barrier, Chaos 2 (1992) 105–115.
[8] N. Hill, Gaussian beam migration, Geophysics 55 (1990) 1416–1428.
[9] L. Hörmander, On the existence and the regularity of solutions of linear pseudo-differential equations, L'Enseignement Math. 17 (1971) 99–163.
[10] E. Kluk, M. Herman, H. Davis, Comparison of the propagation of semiclassical frozen Gaussian wave functions with quantum propagation for a highly excited anharmonic oscillator, J. Chem. Phys. 84 (1986) 326–334.
[11] S. Leung, J. Qian, Eulerian Gaussian beam methods for Schrödinger equations in the semi-classical regime, J. Comput. Phys. 228 (2009) 2951–2977.
[12] S. Leung, J. Qian, R. Burridge, Eulerian Gaussian beams for high frequency wave propagation, Geophysics 72 (2007) SM61–SM76.
[13] S. Leung, J. Qian, S.J. Osher, A level set method for three dimensional paraxial geometrical optics with multiple sources, Commun. Math. Sci. 2 (2004) 657–686.
[14] S.Y. Leung, H.-K. Zhao, Gaussian beam summation for diffraction in inhomogeneous media based on the grid based particle method, Comm. Comp. Phys. 8 (2010) 758–796.
[15] A. Martinez, An Introduction to Semiclassical and Microlocal Analysis, Springer, New York, 2002.
[16] V.P. Maslov, The Complex WKB Method for Nonlinear Equations I Linear Theory, Birkhauser-Verlag, Basel, 1994.
[17] M. Motamed, O. Runborg, Taylor expansion and discretization errors in Gaussian beam superposition, Wave Motion (in press).
[18] P. OĆonnor, S. Tomsovic, E. Heller, Accuracy of semiclassical dynamics in the presence of chaos, J. Stat. Phys. 68 (1992) 131–152.
[19] D. Pathria, J. Morris, Pseudo-spectral solution of nonlinear Schrödinger equations, J. Comput. Phys. 87 (1990) 108–125.
[20] J. Qian, L. Ying, Fast Gaussian wavepacket transforms and Gaussian beams for the Schrödinger equation, J. Comput. Phys. 229 (2010) 7848–7873.
[21] J. Qian, L. Ying, Fast multiscale Gaussian wavepacket transforms and multiscale Gaussian beams for the wave equation, SIAM J. Multiscale Model. Simulat. (in press).
[22] J. Ralston, Gaussian beams and the propagation of singularities, in: W. Littman (Ed.), Studies in Partial Differential Equations, MAA Studies in Mathematics, vol. 23, Mathematical Assn. of America, 1983, pp. 206–248.
[23] N. Tanushev, B. Engquist, R. Tsai, Gaussian beam decomposition of high frequency wave fields, J. Comput. Phys. 228 (2009) 8856–8871.
[24] N. Tanushev, J. Qian, J. Ralston, Mountain waves and Gaussian beams, SIAM J. Multiscale Model. Simulat. 6 (2007) 688–709.
[25] L. Ying, E. Candes, The phase flow method, J. Comp. Phys. 220 (2006) 184–215.